NASA CR-137756
ASRL TR 174-4

A STUDY OF GUST AND CONTROL RESPONSE OF MODEL ROTOR-PROPELLERS IN A WIND TUNNEL AIRSTREAM

Norman D. Ham
Paul H. Bauer
Thomas H. Lawrence
Masahiro Yasue

August 1975

Prepared under Contract No. NAS2-7262 by

Aeroelastic and Structures Research Laboratory
Department of Aeronautics and Astronautics
Massachusetts Institute of Technology
Cambridge, Massachusetts 02139

for

AMES RESEARCH CENTER
NATIONAL AERONAUTICS AND SPACE ADMINISTRATION
MOFFETT FIELD, CALIFORNIA 94035

1. Report No.	2. Government Accession No.	3. Recipient's Catalog No.
NASA CR-137756		

4. Title and Subtitle	5. Report Date
A STUDY OF GUST AND CONTROL RESPONSE OF MODEL ROTOR-PROPELLERS IN A WIND TUNNEL AIRSTREAM	August 1975
	6. Performing Organization Code

7. Author(s)	8. Performing Organization Report No.
Norman D. Ham, Paul H. Bauer, Thomas H. Lawrence, Masahiro Yasue	ASRL TR 174-4
	10. Work Unit No.

9. Performing Organization Name and Address	11. Contract or Grant No.
Massachusetts Institute of Technology Aeroelastic and Structures Research Laboratory Cambridge, Massachusetts 02139	NAS2-7262
	13. Type of Report and Period Covered
12. Sponsoring Agency Name and Address	Contractor Report
National Aeronautics and Space Administration Moffett Field, California 94035	14. Sponsoring Agency Code

15. Supplementary Notes

NASA Technical Monitors: J.P. Rabbott, Jr., and Wayne R. Johnson

16. Abstract

One-ninth-scale model hingeless and gimballed rotor-propellers were tested at an advance ratio of 0.7 in the Wright Brothers Wind Tunnel at MIT, in the presence of sinusoidal longitudinal and vertical gusts produced by a gust generator of novel design. The gimballed rotor was also subjected to sinusoidal collective and cyclic control inputs.

Model test data in terms of blade inplane and out-of-plane bending, longitudinal and lateral gimbal motion, wing vertical and chordwise bending, and blade and wing torsion are presented and compared with theory.

17. Key Words (Suggested by Author(s))	18. Distribution Statement
Rotary Wing Dynamics Gust Response Proprotor Tilt-Rotor	Unclassified, Unlimited

19. Security Classif. (of this report)	20. Security Classif. (of this page)	21. No. of Pages	22. Price*
Unclassified	Unclassified	54	

* For sale by the National Technical Information Service, Springfield, Virginia 22151

FOREWORD

This report has been prepared by the Aeroelastic and Structures Research Laboratory (ASRL), Department of Aeronautics and Astronautics, Massachusetts Institute of Technology, Cambridge, Massachusetts, under NASA Contract No. NAS 2-7262 from the Ames Research Center, National Aeronautics and Space Administration, Moffett Field, California 94035. Mr. John Rabbott and Dr. Wayne Johnson of the Ames Research Center served as technical monitors. The valuable assistance and advice received from these individuals is gratefully acknowledged.

ABSTRACT

One-ninth-scale model hingeless and gimballed rotor-propellers were tested at an advance ratio of 0.7 in the Wright Brothers Wind Tunnel at MIT, in the presence of sinusoidal longitudinal and vertical gusts produced by a gust generator of novel design. The gimballed rotor was also subjected to sinusoidal collective and cyclic control inputs.

Model test data in terms of blade inplane and out-of-plane bending, longitudinal and lateral gimbal motion, wing vertical and chordwise bending, and blade and wing torsion are presented and compared with theory.

CONTENTS

SECTION 1

INTRODUCTION

1.1 General

The tilting proprotor aircraft, one of the composite aircraft family, is a very promising concept that combines into one aircraft the hover efficiency of the helicopter and the high-speed efficiency of the fixed-wing aircraft.

The typical tilting proprotor aircraft is a twin-engine aircraft with tilting rotors mounted on each wing tip. Its configuration consists of a fuselage, a high swept-forward wing, and an empennage. The empennage has a vertical stabilizer and rudder, and a horizontal stabilizer and elevator. The large diameter rotors are three bladed, hingeless or gimbal-type rotors which are mounted on the rotor shaft. The rotor shaft is connected through the gearbox to each engine in the pylon attached at the wing tip. The conversion system provides the rotation of the rotor pylon from the vertical position to the horizontal position and return, in order to obtain the helicopter mode or airplane mode corresponding to the desired flight regime.

When the aircraft takes off or lands, the rotor pylon is rotated to the vertical position to achieve vertical takeoff or landing similar to the helicopter. The flight controls apply pitch changes to the rotor to provide the longitudinal and directional control corresponding to helicopter rotor cyclic pitch, while the collective pitch controls vertical flight and roll motion.

In high-speed flight, the rotor pylon is rotated to a horizontal position similar to that of the conventional propeller type aircraft. The thrust is produced by the rotor, and the lift by the wing. The flight controls are provided by the conventional aircraft control surfaces such as the elevator, rudder and aileron.

The tilting proprotor is exposed to a severe aerodynamic environment including gusts, the wake of preceding blades, and harmonic airloading like a helicopter. But its dynamic and aeroelastic characteristics are in many ways unique; for example, the large flexible blades with a large amount of

twist experience significant coupled out-of-plane (flapping) and inplane (lagging) motion.

As described later in Subsection 1.2, several years of experimental and theoretical analyses have been conducted to establish a fundamental understanding of the dynamic and aeroelastic behavior. However, it is necessary to understand the aeroelastic response of this aircraft to atmospheric turbulence more adequately and to predict it more accurately, since during the preliminary design phase, vibration level prediction is required in order: (a) to evaluate the fatigue life of the blade and wing, (b) to estimate the ride qualities of the vehicle, and, if necessary, (c) to develop suitable gust alleviation devices.

Several design compromise concepts, which make the present analysis distinct from helicopter aeroelastic analysis, are now stated briefly.

In order to obtain high hover efficiency from the rotor, it is desirable to achieve low disc loading, in other words to use large-diameter rotors whose swept discs reach nearly to the fuselage. When the aircraft is operated in high forward speed axial flight in the airplane mode, the rotor is operating at a high inflow ratio (the ratio of axial velocity to blade tip speed). This phenomenon is very different from the helicopter rotor operation which involves low inflow. High inflow operation requires a large built-in angle of twist for efficient cruising. Therefore, significant coupled out-of-plane (flapping) and inplane (lagging) motion occurs in the large, flexible and twisted blade.

The engines and gearboxes are usually located at the wing tip to avoid transmitting high power through a long drive shaft. This leads to low wing natural frequencies and possible resonances in the low frequency range. Also, the center of gravity of the pylon and rotor does not usually coincide with the elastic axis of the wing. Hence, this results in coupled bending and torsion.

1.2 Brief Survey of Past Work

Because VTOL configurations have unconventional propeller-rotor systems, whirl flutter was a major design consideration on present proprotor aircraft.

The analysis presented in Ref. 1 is for a two-bladed rotor free to tilt on a shaft with two nacelle degrees of freedom (pitch and yaw). No

lag or coning degrees of freedom are considered. The analytical method was compared with test results for an existing tilting proprotor aircraft (the Bell XV-3) and of subsequently-tested scale models. They showed good agreement.

Young and Lytwyn in Ref. 2 present a very precise analysis for the whirl stability of a multi-bladed rotor mounted on a nacelle which has pitch and yaw degrees of freedom. Each blade has one flap-wise degree of freedom. The blade mode shape is assumed to be a rigid body mode shape. It was concluded that whirl stability is poorest when the nacelle pitch frequency equals the nacelle yaw frequency, but in this situation nacelle damping is quite effective. There is an optimum value of flap bending frequency somewhere between 1.1 and 1.35 for highly stabilized whirl motion.

This analysis neglects the effect of coning on proprotor aerodynamics, and flap bending mode shapes other than the rigid blade mode used. Also, autorotation flight must be considered as well as powered flight.

In Ref. 3, Gaffey points out that a highly coupled blade mode has substantial flap bending even if the primary mode involves in-plane motion. This occurs in the case of a highly twisted blade or a blade operating at high geometric pitch angles such as a proprotor blade. The analysis shows that a moderate amount of negative δ_3 (flapping angle at the blade root gives the pitch angle reduction of the amount $\beta \tan \beta_3$ if δ_3 is positive) has a stabilizing influence on proprotors subject to flap-lag instability at high inflows.

Preliminary design studies of prototype vehicles (Refs. 4 and 5) as a part of the current NASA/ARMY sponsored tilting proprotor research aircraft program give some results from dynamic and aeroelastic analyses done by Bell and Vertol.

Johnson, Refs. 6 and 7, derived the equations of motion for a cantilever wing with the rotor at the wing tip. He develops a nine degree-of-freedom model which involves blade flapping motion and lagging motion (each has one collective and two cyclic motions, respectively), wing vertical bending, chordwise bending, and torsion. This model is applied to two proprotor designs and compared with the results of some full-scale wind tunnel tests. It shows reasonable correlation between theory and experiment.

Yasue, Ref. 8, developed equations of motion for a rotor-propeller aircraft in cruising flight and implemented them in a computer program, Ref. 9. The formulation is based on Galerkin's method using coupled mode shapes for the blade and wing. This procedure is applied to the analysis of two types of rotors, gimballed rotor and hingeless. The results are evaluated by means of eigenvalue analysis of the stability of the system and frequency response analysis of the gust and control response.

1.3 Objectives of the Present Study

The objective of this study is to establish a verified method of predicting the dynamic and aeroelastic behavior of the tilting proprotor aircraft.

The equations of motion for a cantilever wing with a rotating rotor at the wing tip were derived as consistently as possible in Ref. 8. The great complexity of rotor blade motion was included by accounting for blade rotation (i.e., centrifugal and Coriolis forces), significant inplane motion, and the large twist and high pitch angles at high inflows.

The resulting system of equations, obtained using modal analysis, are applied to the analysis of experimental results obtained by testing two model proprotor configurations (one is a hingeless, soft-inplane type rotor and the other is a gimballed, stiff-inplane rotor : Reference 10.) The tests were conducted in the MIT Wright Brothers Wind Tunnel using the gust generator described in Reference 11. The proprotors were operated in autorotation, which is shown to be a close approximation to powered operation in Ref. 12.

SECTION 2

MODEL DESCRIPTION, INSTRUMENTATION, AND TEST PROCEDURES

2.1 Model Description

The model is a semi-span, Froude scaled, unpowered tilt rotor with a diameter of 33.75 inches. (See Figure 1). It provides a dynamic simulation of either a 26-foot diameter three-bladed hingeless tilt rotor system (scale factor = 1/9.244) or a 25-foot, three-bladed, gimballed rotor system (scale factor = 1/8.888). A high performance closed-loop proportional control system is provided for collective pitch and two orthogonal components of cyclic pitch. A fully mass-balanced aerodynamic forcing vane driven by a constant velocity servo loop is included for model forcing. Both the rotor blades and wing are fully strain-gage instrumented.

A separate, special purpose electronic controller is used to drive the collective and cyclic servos and forcing vane. In addition, the controller contains a patchable analog computer which allows signals originating in any part of the model to be used in a closed-loop manner to control swash plate tilt.

Precise Froude scaling could not be rigidly adhered to, but similarity of natural frequencies has been maintained in order to preserve dynamic similarity.

The model parameters are listed in Appendix A. The wing is composed of a one-inch by one-half-inch solid aluminum spar covered by a two-piece molded fiberglas fairing. The bottom of the spar fits with a 5.5-degree forward sweep into a mounting pedestal, while the top carries the nacelle attachments. Since the two rotor systems require different wing natural frequencies, tip weights are added to the top of the spar in the hingeless rotor configuration. The spar carries beamwise, chordwise, and torsional bending gages at the 5% and 79% semi-span positions.

The nacelle exterior consists of upper and lower molded fiberglas fairings. Carried inside the nacelle are: rotor shaft, swash plates,

cyclic and collective servo actuators, slip rings, one-per-rev pulser, rotor shaft tachometer, forcing vane motor, forcing vane tachometer, and gimbal position potentiometers (used only with the gimballed rotor).

The cyclic actuators are 90-degrees apart and each drives a lead screw to control swash-plate tilt. The entire cyclic control assembly rides on a pair of lead screws driven by the collective actuator.

Rotating system instrumentation wires run inside the hollow rotor shaft to a 38-channel slip ring mounted at the rear of the nacelle.

The forcing vane has an area of 8.75-square inches and is a symmetric 0012 section. It can oscillate through either $\pm$ 5 or $\pm$ 10 degrees. The vane is driven by a D.C. motor and balanced crank.

The hingeless rotor blades are constructed of epoxy resin impregnated glass fiber over a 4 lb/ft^3 foam core. The spar is rectangular inboard, transitioning to a 'D' spar at r/R = 0.45. The inboard section is solid epoxy-impregnated glass fiber, with instrumentation leads imbedded inside. The blade skin inboard of r/R = 0.45 is not load-bearing and can be removed for access to blade instrumentation. Aluminum pitch horns are secured to steel root fittings. A cylindrical cavity is provided at each blade tip for small tuning weights used to match blade frequencies.

The hub is a single piece of machined aluminum, incorporating 2.5 degrees of precone and 0.070 inches of torque offset.

Each blade has flapwise and chordwise bending strain gages at r/R = 0.08 and a torsional bending gage at r/R = 0.10. Additionally, No. 3 blade has outboard instrumentation consisting of flapwise and chordwise gages at r/R = 0.42 and a torsional gage at r/R = 0.44.

The gimballed rotor blades are constructed similarly to those of the hingeless rotor, except that the spar is a hollow box section of preimpregnated glass cloth and the aft skin is stabilized with 0.012-inch balsa sheet. In this case, the entire blade skin is load carrying. Aluminum pitch horns are bonded integrally into the spar.

The same molds were used for both types of blades, resulting in small

out-of-scale effects in chord and twist distribution for the gimballed rotor.

The gimballed rotor hub consists of a free-swivelling hub carrying the blades and a rotating gimbal, an outer fixed gimbal, three flap-restraining springs and a spring retainer. Two links, 90 degrees apart, connect the outer gimbal with the gimbal position potentiometers in the nacelle. The hub incorporates 1.5 degrees of precone.

All three blades are instrumented inboard and outboard, with flapwise and chordwise gages at r/R = 0.11 and 9.30, and torsional gages at r/R = 0.12 and 0.29. A spare chordwise gage is provided at r/R = 0.30 because of the inaccessibility of the outboard gage.

The model controller contains three servo-amplifiers to drive the cyclic and collective actuators, the forcing vane controller, and the patchable analog computer (see Figure 2).

The servo-amplifiers are fully solid state, providing D.C. control signals and receiving feedback potentiometer position voltages. Thus, each actuator is provided with an independent closed-loop positioning servo-mechanism. Command signals can be generated manually through digital potentiometers or automatically through the analog computer. The analog computer contains summing amplifiers, inverters, buffers, switches, and a phase shifter, all accessible through patching bays. Various control laws can be easily implemented. In this way, strain-gage signals from any part of the model can be mixed and phased to drive the servo-actuators.

2.2 Determination of Natural Frequencies

Static natural frequencies of the wing and all rotor blades, both chordwise and flapwise, were determined experimentally with cantilevered hub restraint. These tests verified the model design and provided values for incorporation into a computer model of the system.

Table 1 gives frequency values for the wing. The two rotor systems require different wing frequencies, shown by the two sets of entries.

Full-scale frequencies were taken from experimental data on full-scale models and then scaled down (Columns 1 and 2). Column 3 is the actual model value and Column 4 the corrected computer model value. Hingeless rotor wing chordwise frequency could not be determined due to coupling between wing chordwise and blade-flapping modes.

Table 2 lists hingeless rotor blade frequencies. Values for the full-size rotor were calculated from stiffness and mass distribution data and then scaled. Columns 1 and 2 give these values while Column 3 gives the model values (lowest and highest blade) and the corrected computer value.

Data for the gimballed rotor were treated as for the hingeless rotor in Table 3. In addition, experimental full-size values were available and were also scaled down (Columns 5 and 6).

2.3 Test Instrumentation

The primary purpose of these tests was to determine the model response to vertical and longitudinal gusts. Stability tests were also run on both models, while the gimballed rotor version was tested for its response to sinusoidal control inputs.

Gust response was measured by an RMS voltmeter switched to the appropriate strain gage. The stability of the wing vertical bending mode was investigated by exciting the model and then observing the decay rate.

Since the model was being operated in a harsh environment, oscilloscopes were used to monitor blade and wing stresses. Flapwise and chordwise signals from the Number 3 blade inboard gages were fed into the vertical and horizontal axes of an oscilloscope to form a Lissajou's figure. This display was monitored to ensure that the imposed stresses did not exceed the allowable values. The wing stresses were monitored in a similar manner.

For final tests, the blade display monitored the outboard gages (30% radius) at the critical station, while the second display monitored gimbal position instead of wing stresses.

A 12-channel oscillograph was also used. During the gust response tests, the following inputs were recorded: wing flapwise, chordwise, and torsion; blade flapwise, chordwise, and torsion; pitch and yaw gimbal position; one-per-rev pulses from the rotor shaft and from the generator. For the

TABLE 1

WING NATURAL FREQUENCIES (Hz), HUB AND BLADES PRESENT

MODE \ SOURCE	Exper. Full-Size Model 1	Scaled Full-Size Model 2	Actual Model 3	Corrected Computer Model 4
Hingeless Rotor				
Beamwise	2.3	6.99	7.43	8.04
Chordwise	4.0	12.2	--	13.9
Torsion	9.2	28.0	36.3	36.3
Gimballed Rotor				
Beamwise	3.2	9.54	8.10	8.6
Chordwise	5.35	15.9	13.2	14.8
Torsion	9.95	29.7	33.3	31.2

TABLE 2

HINGELESS ROTOR NATURAL FREQUENCIES (H_z)

MODE \ SOURCE	Calculated Full Size 1	Scaled Full Size 2	Actual Model 3	Corrected Computer Model 4
Flapwise	3.0	9.11	8.57-9.46	9.0
Chordwise	4.94	15.0	14.3-15.7	15.4

TABLE 3

GIMBALLED ROTOR NATURAL FREQUENCIES (Hz)

SOURCE / MODE	Calculated Full Size 1	Scaled Full Size 2	Actual Mode 3	Corrected Computer Model 4	Full Size Exper. 5	Scaled Full Size Exper. 6
Flapwise	7.11	21.2	22.5-23.6	21.7	7.5	22.4
Chordwise	17.3	51.7	39.0-41.7	36.1	12.2	36.4
Torsion	--	--	233-250	--	--	--

control response tests, the gust generator pulse was deleted, and two new inputs added: one for the servo-command signal, the other for the servo-response (followup pot) signal.

2.4 Test Procedures

For the gust and control tests, the model was run at constant tunnel speed and rotor rpm while being excited by either gusts or control inputs of increasing frequency. At each frequency, RMS voltage measurements were made of all three wing signals and blade flapwise and chordwise signals. During tests on the gimballed rotor, blade torsion and gimbal position signals were also measured, and the followup pot signal was measured during the control tests.

Tests were conducted in autorotation at 82.5 mph and 1200 rpm (advance ratio 0.7) for the hingeless rotor. Vertical and longitudinal gusts of RMS amplitude 1.5% of free stream were varied from 200 to 900 cpm in 100 cpm increments, with finer increments near resonances.

Tests were conducted in autorotation at 95 mph and 1360 rpm (advance ratio 0.7) for the gimballed rotor. Vertical and longitudinal gusts of RMS amplitude 2.0% and 2.5% of free stream, respectively, were varied from 300 to 1400 cpm in 100 and 200 cpm increments. Control inputs were varied from 300 to 930 cpm in 90 cpm increments. In both cases, finer increments were taken near resonances. Oscillograph records were taken along with RMS voltmeter signal readings.

SECTION 3

DISCUSSION OF RESULTS AND COMPARISON WITH THEORY

3.1 Hingeless Rotor Gust Response

The hingeless rotor model described in Section 2 and in Reference 10 was subjected to sinusoidal longitudinal and vertical gusts at various frequencies (Figure 3), at a wind tunnel velocity of 82.5 miles per hour, and with a rotor rotational speed of 1200 revolutions per minute. This test case corresponded to full-scale operation at an advance ratio of 0.7. Model response was measured in terms of blade inplane and out-of-plane bending motion, wing vertical and chordwise bending, and wing torsion.

Test results are presented in Figures 5 and 6. Also shown are theoretical predictions of the model response using the method of Refs. 8 and 9. In comparing theory with experiment, it was necessary to add "tare" RMS values of model motion due to tunnel turbulence, measured with the gust generator shut down, to the theoretical values. The RMS magnitude of the tare value used in each case is indicated by an arrow at the left axis of each figure.

For the longitudinal gust case, Figure 5, agreement is seen to be fairly good except in the vicinity of the resonance peaks, where structural damping not accounted for in the theory reduced the experimental values.

For the vertical gust case, Figure 6, the theory underpredicts the blade responses, while the wing vertical bending response is reduced by structural damping not accounted for in the theory.

The discrepancy between theory and experiment for the blade bending responses is believed to be due to difficulties in representing the blade root boundary conditions in the theoretical calculation of the coupled blade bending mode shapes.

Wing vertical bending response to longitudinal gusts, wing chordwise bending response to vertical gusts, and wing torsional response to both types of gust are not shown since these responses were negligible, both

experimentally and theoretically.

3.2 Gimballed Rotor Gust Response

The gimballed rotor model described in Section 2 and in Ref. 10 was subjected to sinusoidal longitudinal and vertical gusts at various frequencies (Figure 3) at a wind tunnel velocity of 95 miles per hour, and with a rotor rotational speed of 1360 revolutions per minute. This test case corresponded to full-scale operation at an advance ratio of 0.7. Model response was measured in terms of blade inplane and out-of-plane bending motion, longitudinal and lateral gimbal motion, wing vertical and chordwise bending, and blade and wing torsion.

Test results are presented in Figures 7 and 8. Also shown are theoretical predictions of the model response using the method of Refs. 8 and 9. In comparing theory with experiment, it was necessary to add "tare" RMS values of model motion due to tunnel turbulence, measured with the gust generator shut down, to the theoretical values. The RMS magnitude of the tare value used in each case is indicated by an arrow at the left axis of each figure.

For both gust cases, the theory underpredicts the blade bending responses, Figures 7(a), 7(b) and 8(a) and 8(b), while the wing bending responses are reduced by structural damping not accounted for in the theory, Figures 7(e) and 8(e).

In Fig. 7(e), the wing chordwise bending response to the longitudinal gust has a small peak at 0.29 per revolution. It was observed from the oscillograph trace that this chordwise response had a frequency which was the same as the wing chordwise natural frequency. It was also confirmed that the peak was largest when the gust frequency was one-half the wing chordwise bending natural frequency. Therefore, it is believed that this second harmonic vibration is due to a second harmonic component of the gust waveform.

The discrepancy between theory and experiment for the blade bending responses is believed to be due to difficulties in representing the blade root boundary conditions in the theoretical calculation of the coupled blade bending mode shapes, and to difficulties in blade bending strain-gage calibration.

The theory overpredicts the gimbal motion response to wing chordwise bending motion excited by longitudinal gusts, Figs. 7(c) and 7(d), presumably due to the reduction of wing bending response by structural damping not accounted for in the theory, and the further reduction of blade flapping response by high friction in the gimbal potentiometers. The increase in the experimental gimbal response at the higher frequencies is believed to be due to blade imbalance (1/rev. in the rotating system) exciting the rotor precession mode (about 2/rev. in the non-rotating system); an increasing 2/rev. signal was seen in the gimbal oscillograph record as gust frequency approached 1/rev.

The theory predicts the gimbal motion response to vertical gusts fairly well, as seen in Figs. 8(c) and 8(d). The apparent increase in the experimental lateral gimbal response at the higher frequencies is due to an increase in the noise level of the RMS voltage signal from the gimbal potentiometer due to a loose wire.

Wing vertical bending response to longitudinal gusts, wing chordwise bending response to vertical gusts, and blade and wing torsional responses to both types of gust are not shown since these responses are negligible, both experimentally and theoretically.

3.3 Gimballed Rotor Control Response

The gimballed rotor model described in Section 2 and in Reference 10 was subjected to sinusoidal collective and cyclic control (Fig. 4) at various frequencies, at a wind tunnel velocity of 95 miles per hour, and with a rotor rotational speed of 1360 revolutions per minute. This test case corresponded to full-scale operation at an advance ratio of 0.7. Model response was measured in terms of blade inplane and out-of-plane bending motion, longitudinal and lateral gimbal motion, wing vertical and chordwise bending, and blade and wing torsion.

Test results are presented in Figures 9 and 10. Also shown are theoretical predictions of the model response using the method of Refs. 8 and 9. In comparing theory with experiment, it was necessary to add "tare" RMS values of model motion due to tunnel turbulence to the theoretical values. The RMS magnitude of the tare value used in each case is indicated by an arrow at the left axis of each figure.

For the collective pitch case, Figure 9, agreement is seen to be fair except in the vicinity of the resonance peaks, where structural damping not accounted for in the theory reduced the experimental values.

For the cyclic control case, the theory underpredicts the blade bending responses in Figures 10(a) and 10(b). The discrepancy between theory and experiment for the blade bending responses is believed to be due to difficulties in representing the blade root boundary conditions in the theoretical calculation of the coupled blade bending mode shapes, and to difficulties in blade bending strain-gage calibration.

For the cyclic control case, the theory overpredicts the gimbal responses in Figures 10(c) and 10(d). It is believed that the significant difference between theory and the experiment resulted from the high friction in the gimbal potentiometers.

The good agreement of the wing vertical bending response to cyclic control in Fig. 10(e) is somewhat fortuitous, since the theoretical response to cyclic control should be considerably larger at resonance than the experimental response if structural damping is neglected.

Wing vertical bending response to collective control, wing chordwise bending response to cyclic control, and blade and wing torsional response to both types of control are not shown since these responses were negligible, both experimentally and theoretically.

SECTION 4

CONCLUSIONS

The present study had two primary objectives. The first objective was the acquisition of gust response test data for use in the design of a gust alleviation system for proprotor aircraft. The second objective was the correlation of this test data with a previously developed ten degree-of-freedom theory (Refs. 8 and 9).

It was found that,in general, the theory adequately predicted the test data. As would be expected, structural damping present in the model greatly reduced the magnitudes of resonant responses from those predicted by the theory. The difficulty of correctly representing the coupled blade bending mode root boundary conditions led to discrepancies between theory and test in the blade bending response. Finally, the random turbulence present in the wind tunnel produced a "tare" RMS response of the model which could be accounted for only approximately in the comparison between theory and test, leading to some small degree of error.

It is believed that the theory in its present form gives a reasonable representation of proprotor gust and control response at an advance ratio of 0.7.

REFERENCES

1. Hall, E.W. Jr., "Prop-Rotor Stability at High Advance Ratios". Journal of American Helicopter Society, Vol. 11, No. 2, 1966, pp. 11-26.

2. Young, M.I. and Lytwyn, R.I., "The Influence of Blade Flapping Restraint on the Dynamic Stability of Low Disk Loading Propeller-Rotors", Journal of American Helicopter Society, Vol. 2, No. 4, 1968, pp. 38-54.

3. Gaffey, T.M., "The Effect of Positive Pitch-Flap Coupling on Rotor Blade Motion Stability and Flapping". Journal of American Helicopter Society, Vol. 14, No. 2, 1969, pp. 49-67.

4. Bell Helicopter Company, "V/STOL Tilt-Rotor Study Task II -- Research Aircraft Design". NASA CR 114442, March 1972.

5. Boeing Vertol Company, "V/STOL Tilt-Rotor Aircraft Study Volume II -- Preliminary Design of Research Aircraft". NASA CR 114438, March 1972.

6. Johnson, W., "Dynamics of Tilting Proprotor Aircraft in Cruise Flight". NASA TN D-7677, May 1974.

7. Johnson, W., "Theory and Comparison with Tests of Two Full-Scale Proprotors". Proceeding of the AHS/NASA-Ames Specialists' Meeting on Rotorcraft Dynamics, Feb. 1974.

8. Yasue, M., "A Study of Gust Response for a Rotor-Propeller in Cruising Flight", NASA CR-137537, August 1974.

9. Yasue, M., "User's Manual for Computer Program ROTOR", NASA CR-137553, August 1974.

10. Nicely J., and Walsh, G., "Technology Data, Operations and Maintenance Manual for a Wind Tunnel Model of a Proprotor and Cantilever Wing", Boeing Document D210-10961-1, June 1975.

11. Ham, N.D., Bauer, P.H., and Lawrence, T.H., "Wind Tunnel Generation of Sinusoidal Lateral and Longitudinal Gusts by Circulation Control of Twin Parallel Airfoils", NASA CR-137547, August 1974.

12. Johnson, W., "The Influence of Engine/Transmission/Governor on Tilting Proprotor Aircraft Dynamics", NASA TM X-62455, June 1975.

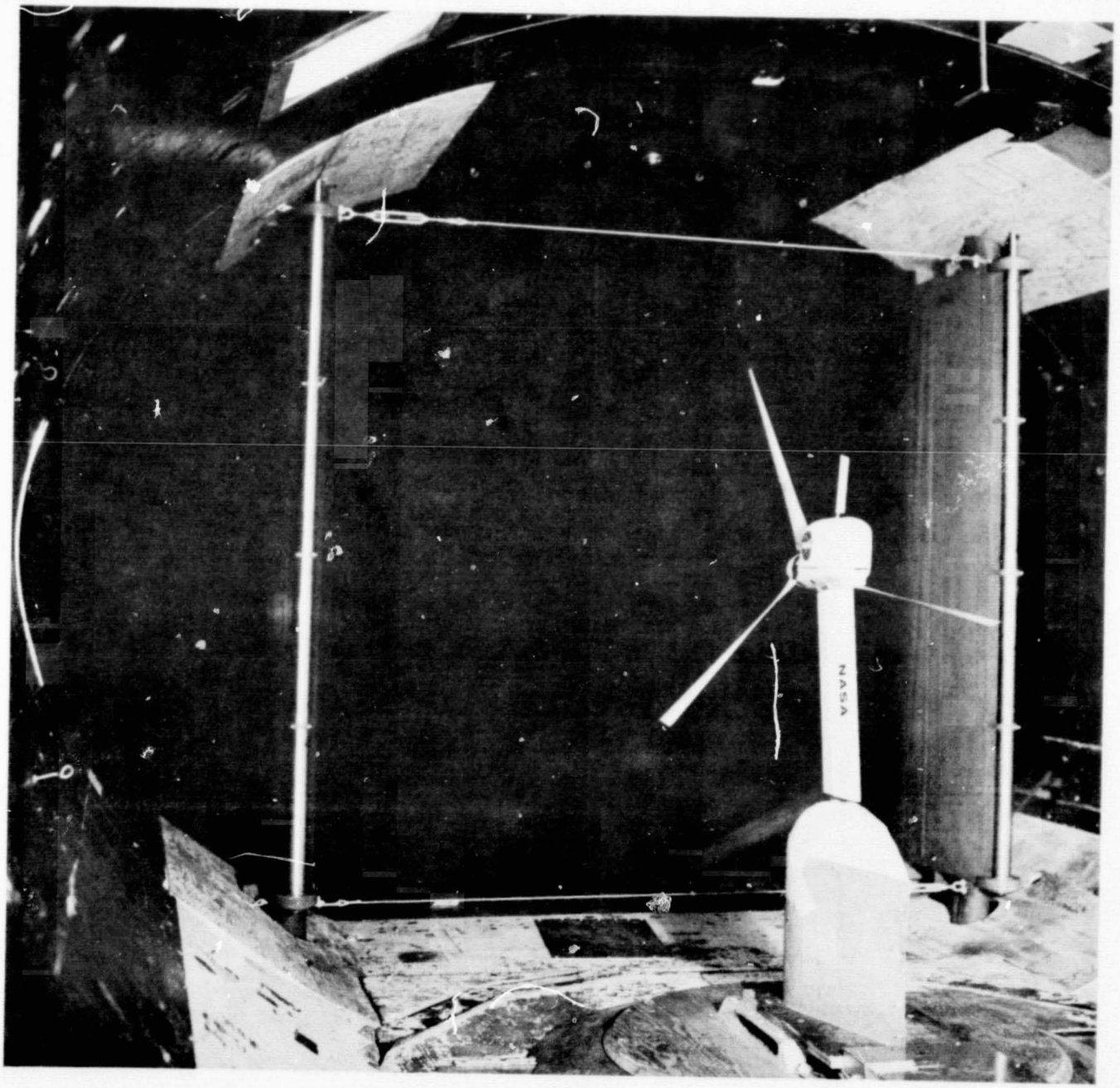

FIG. 1 MODEL SHOWN MOUNTED IN WIND TUNNEL WITH GUST GENERATOR IN BACKGROUND

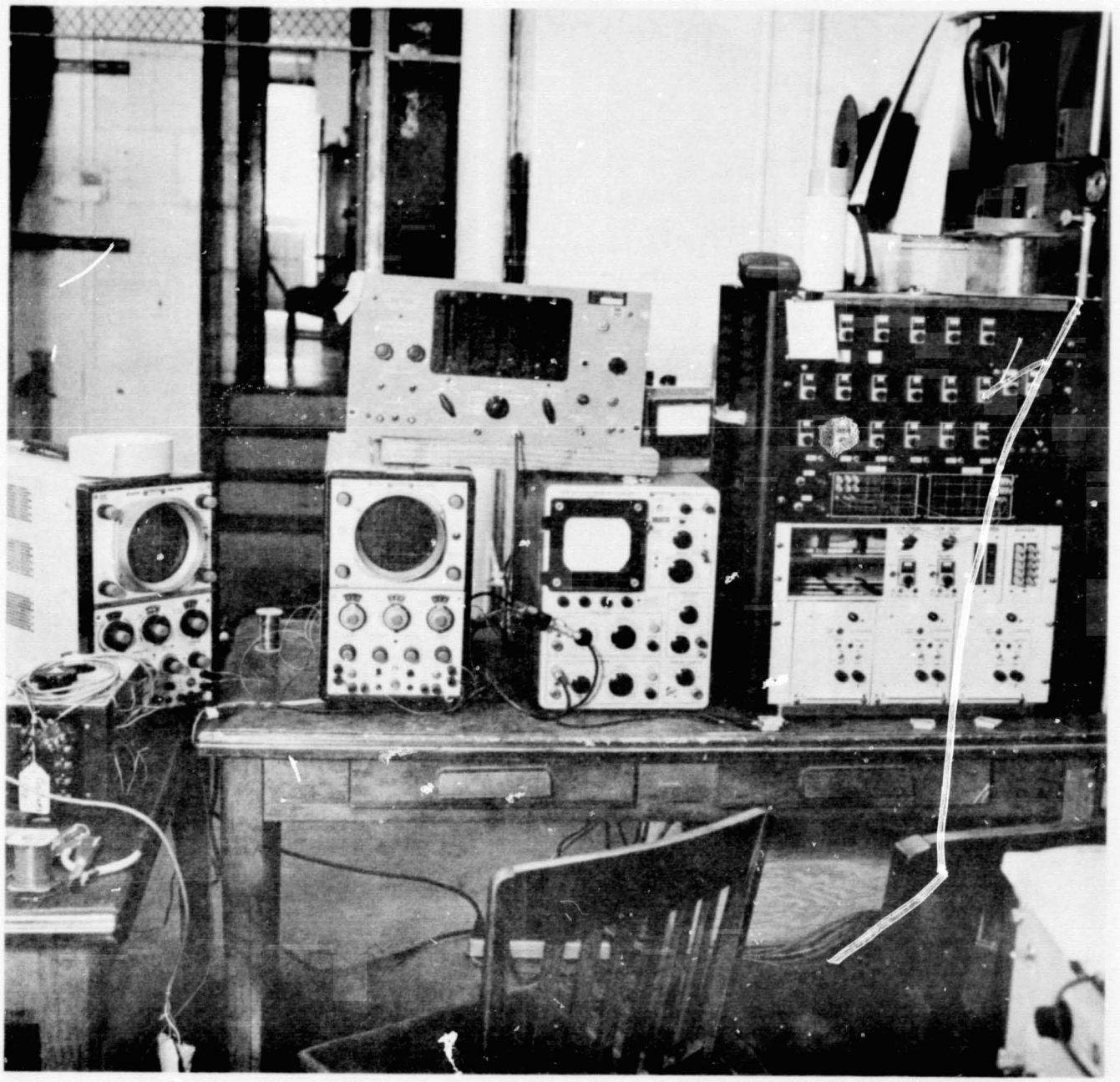

FIG. 2 MODEL OPERATOR'S STATION SHOWING CONTROL PANEL AND INSTRUMENTATION

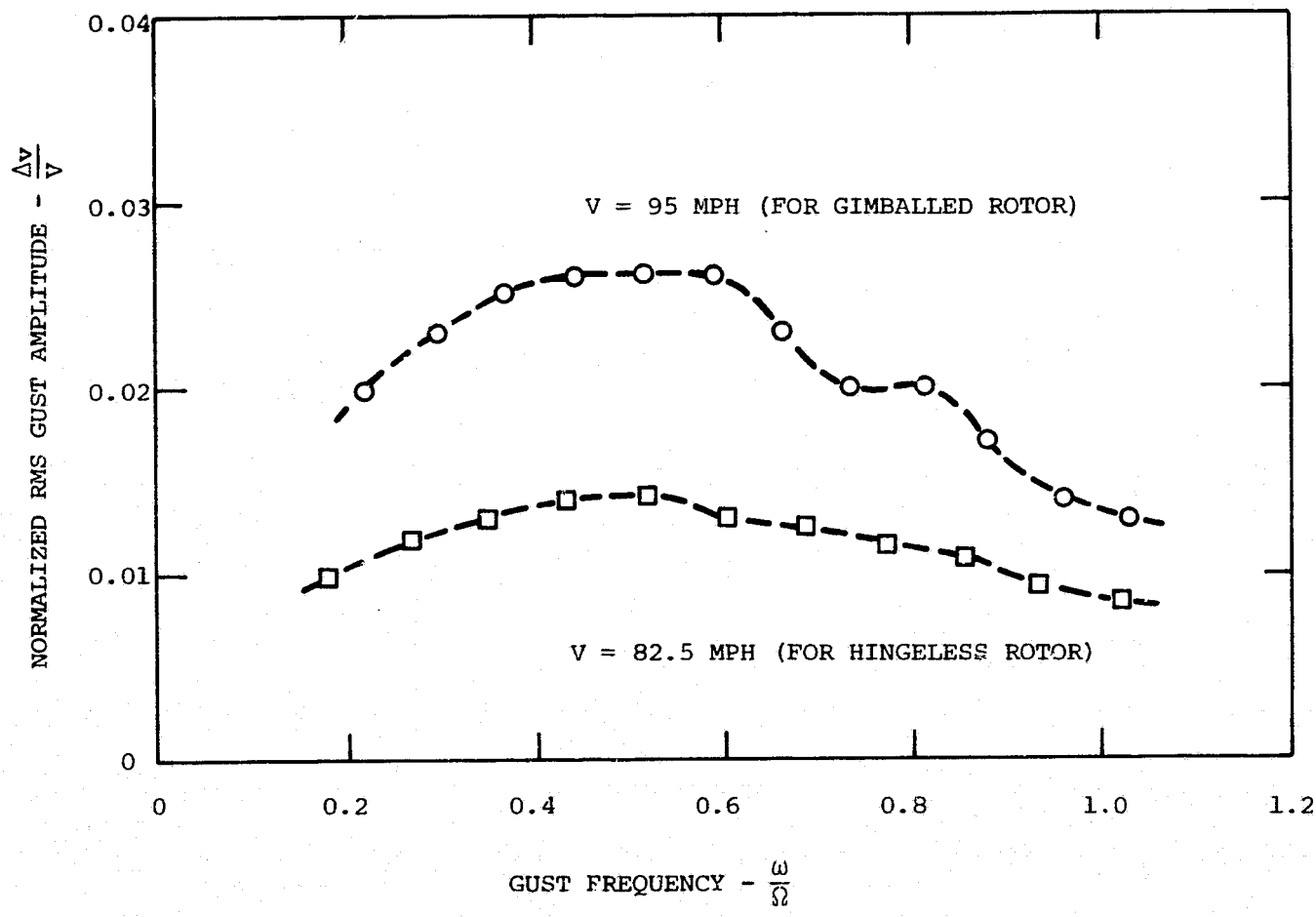

FIG. 3(a) LONGITUDINAL GUST AMPLITUDE

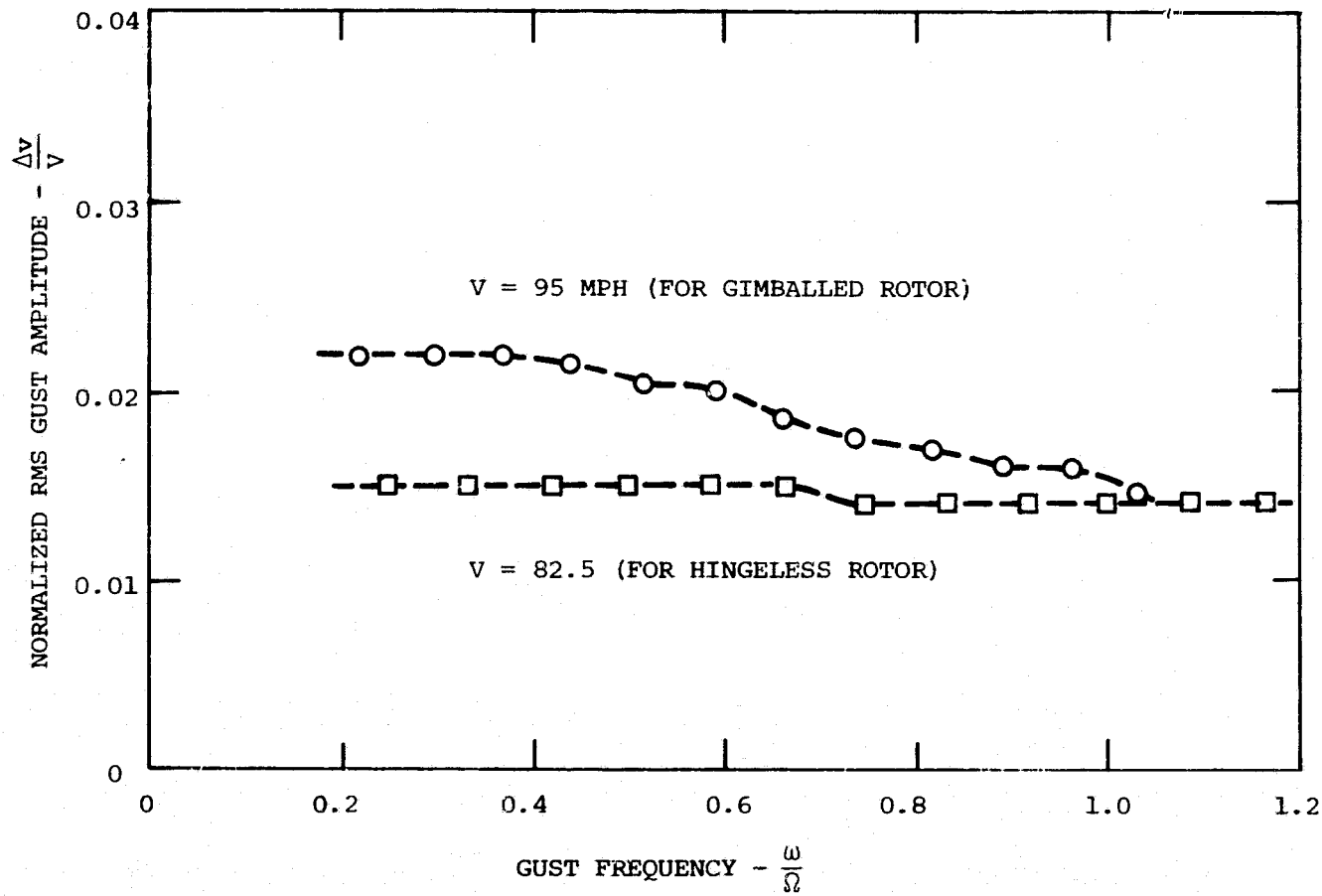

FIG. 3(b) VERTICAL GUST AMPLITUDE

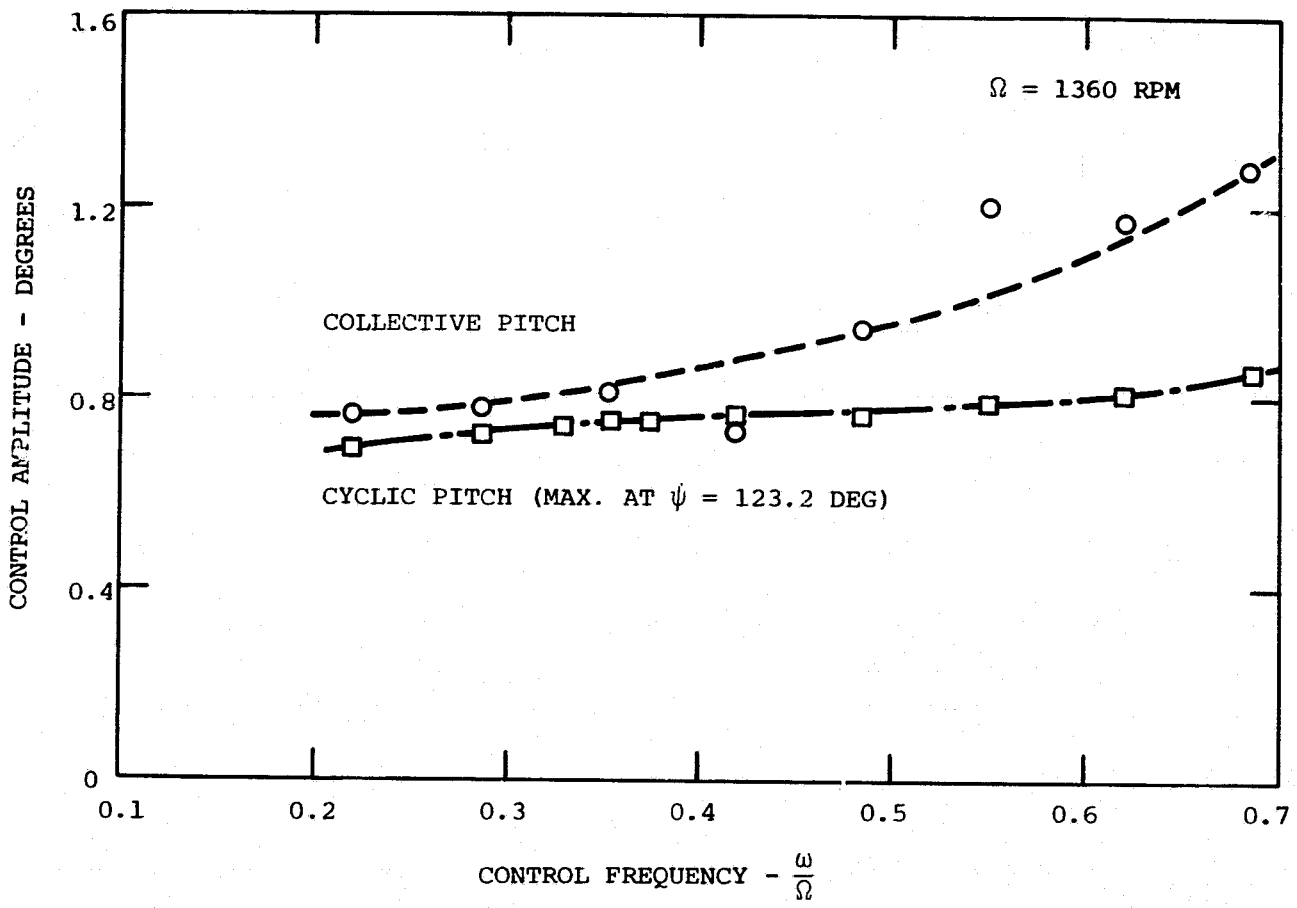

FIG. 4 COLLECTIVE AND PORT ACTUATOR CYCLIC PITCH AMPLITUDE (GIMBALLED ROTOR)

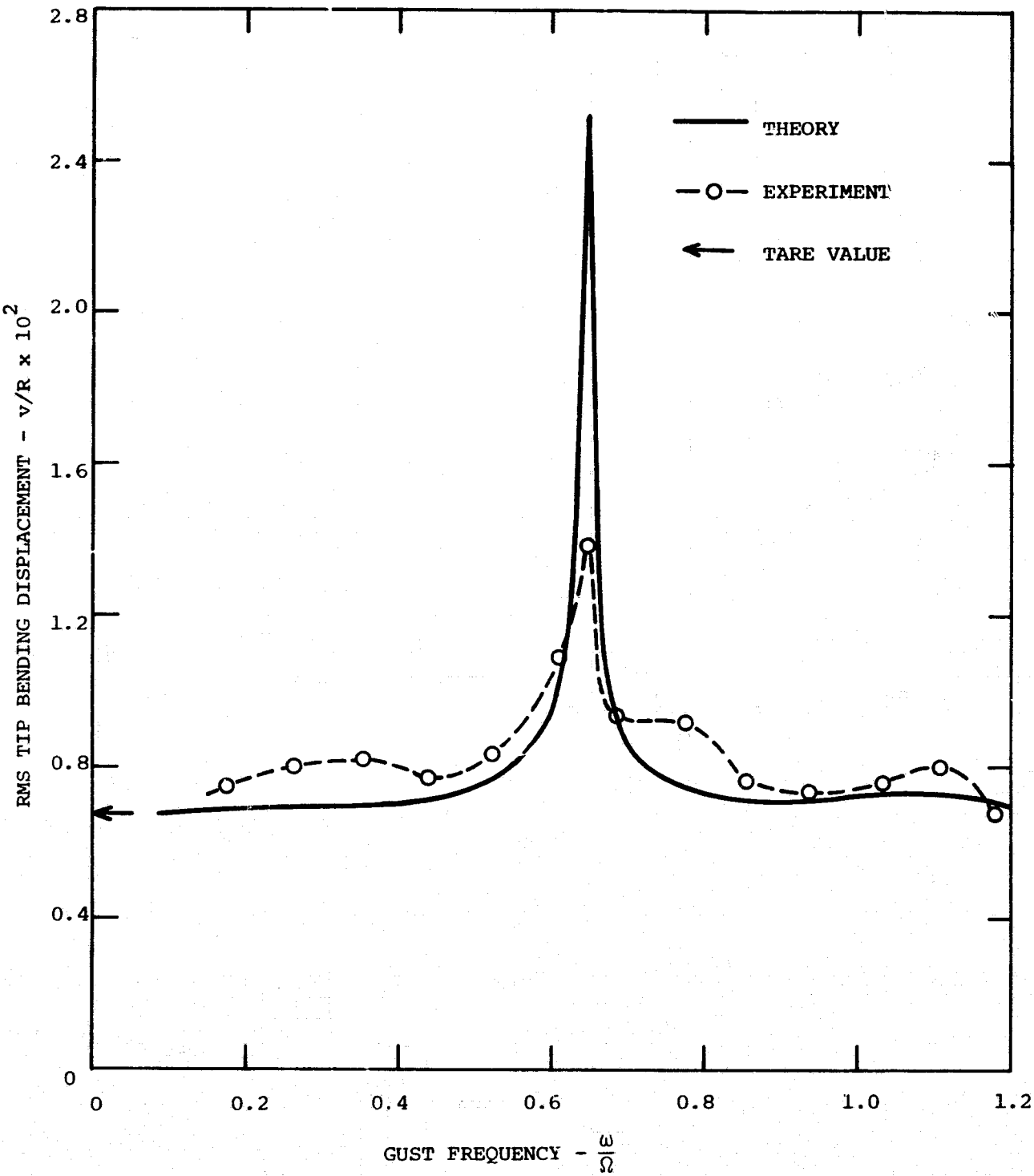

FIG. 5(a) LONGITUDINAL GUST RESPONSE OF HINGELESS ROTOR BLADE INPLANE BENDING

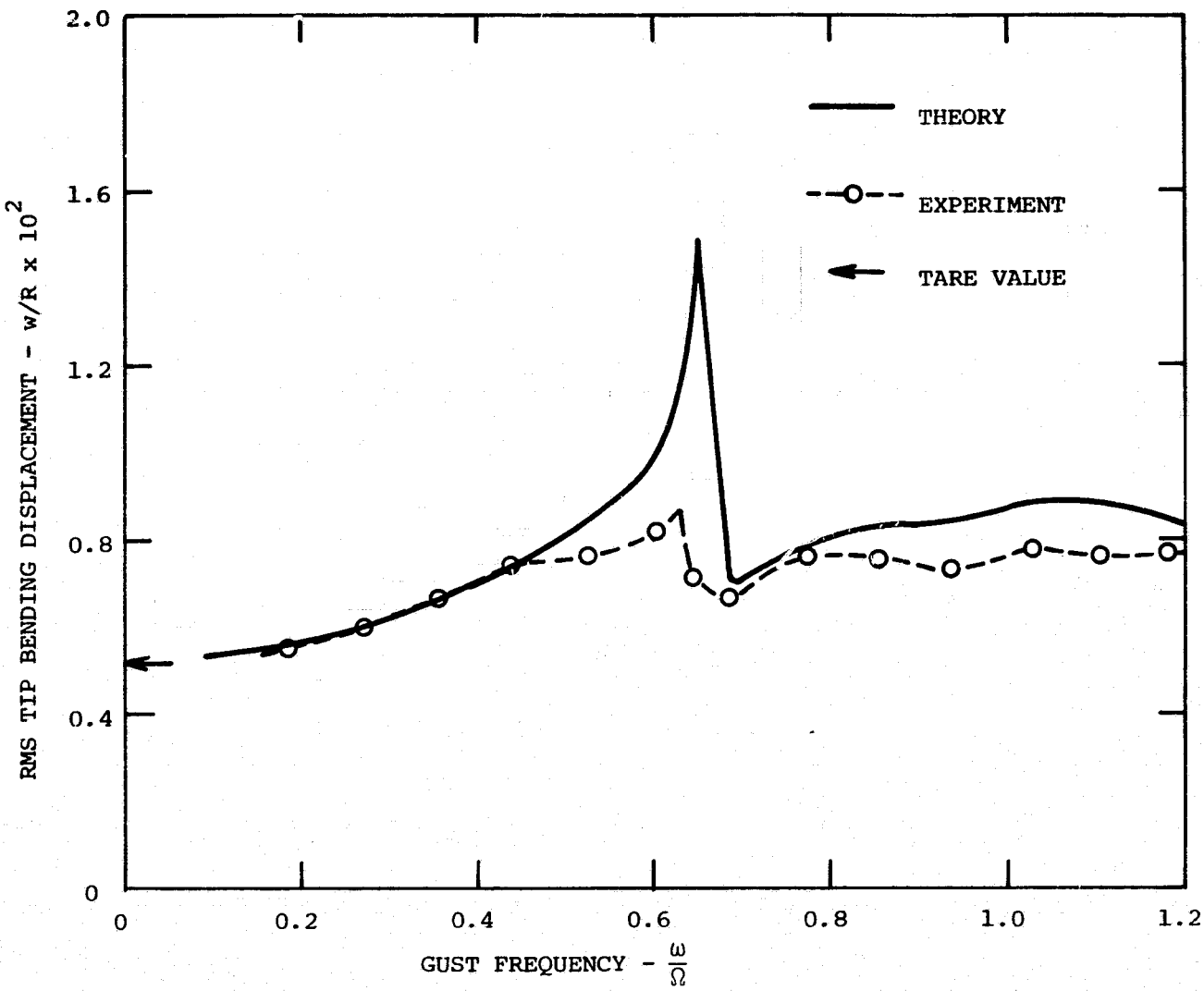

FIG. 5(b) LONGITUDINAL GUST RESPONSE OF HINGELESS ROTOR BLADE OUT-OF-PLANE BENDING

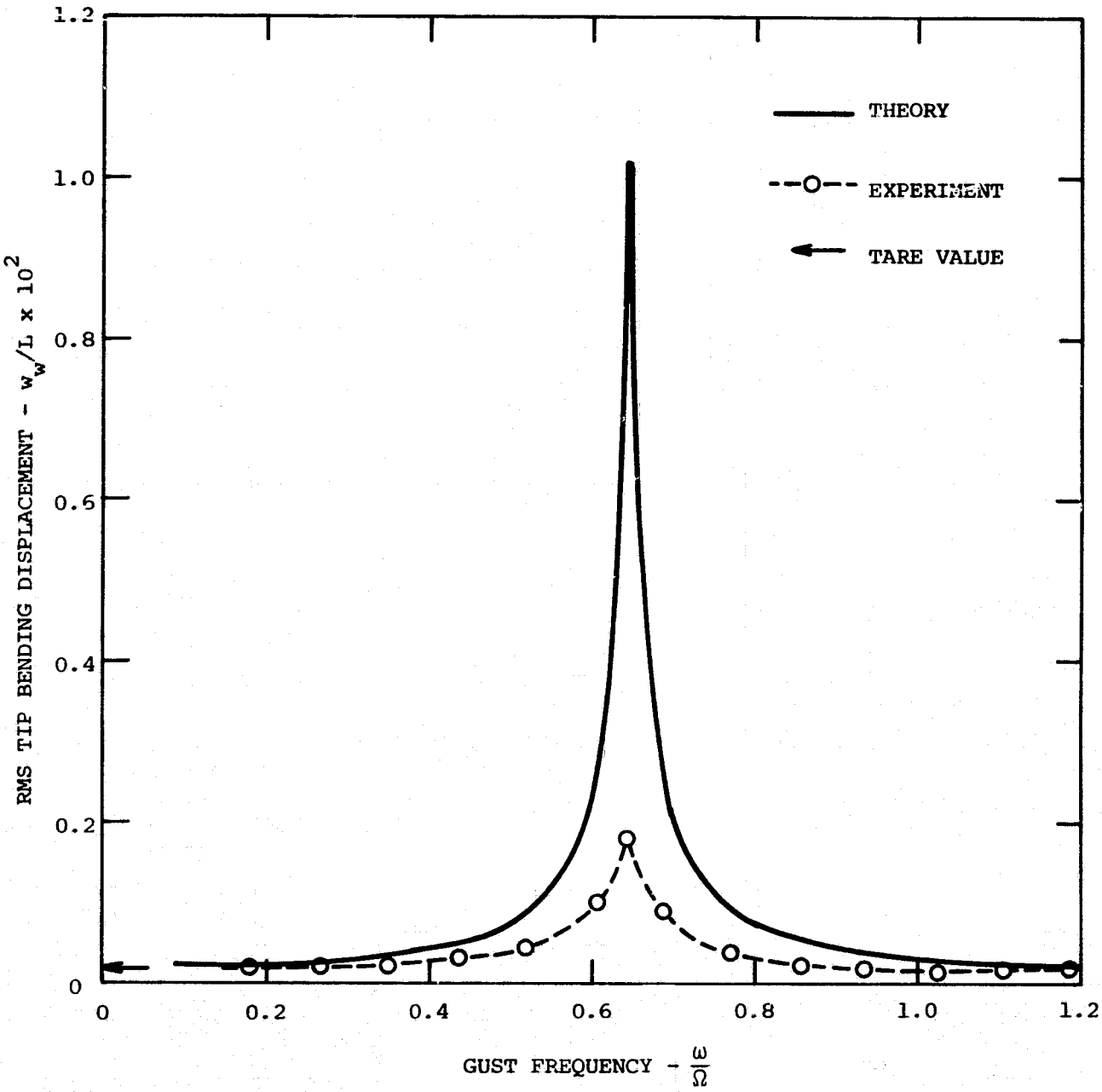

FIG. 5(c) LONGITUDINAL GUST RESPONSE OF HINGELESS ROTOR WING CHORDWISE BENDING

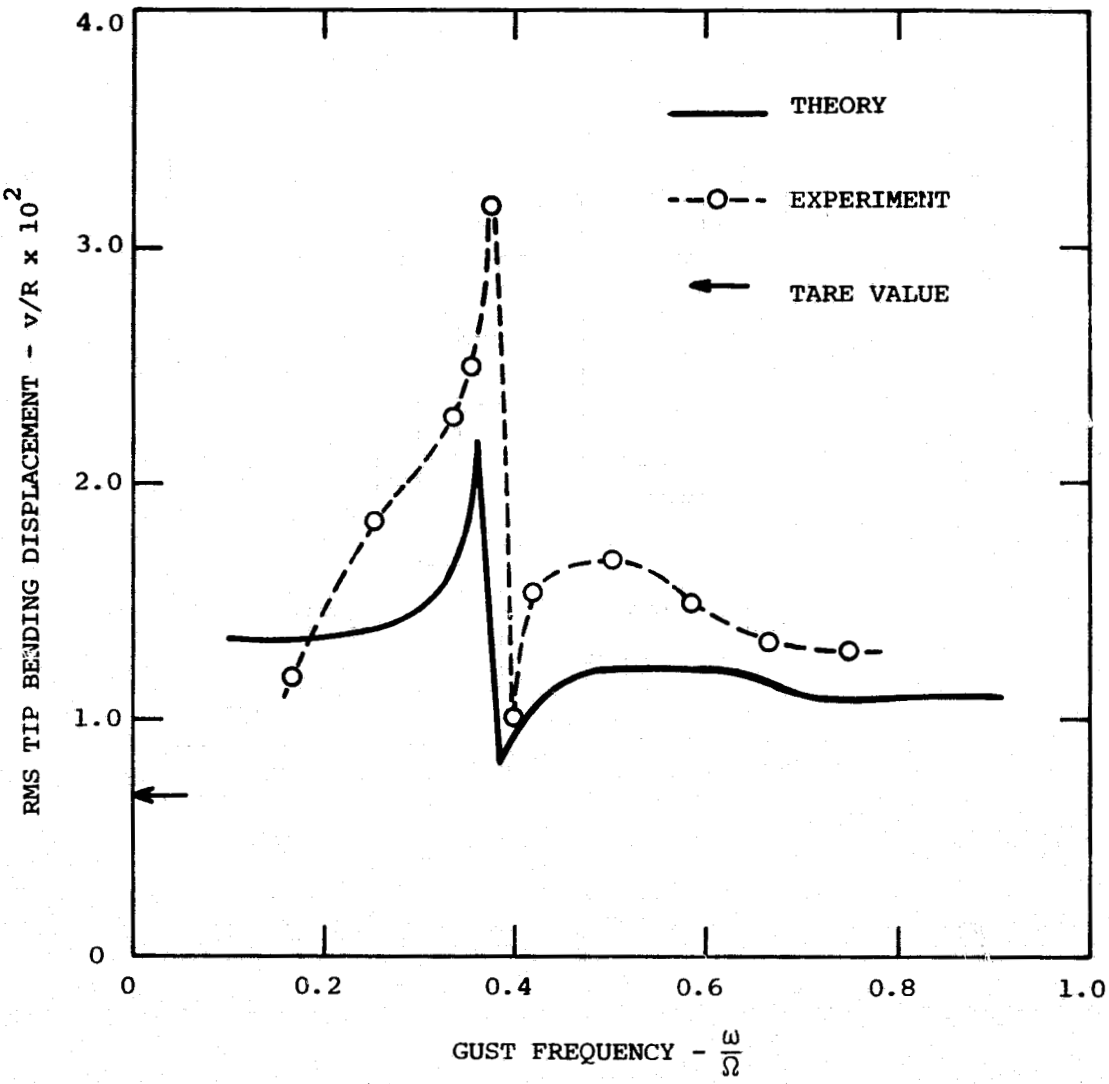

FIG. 6(a) VERTICAL GUST RESPONSE OF HINGELESS ROTOR BLADE INPLANE BENDING

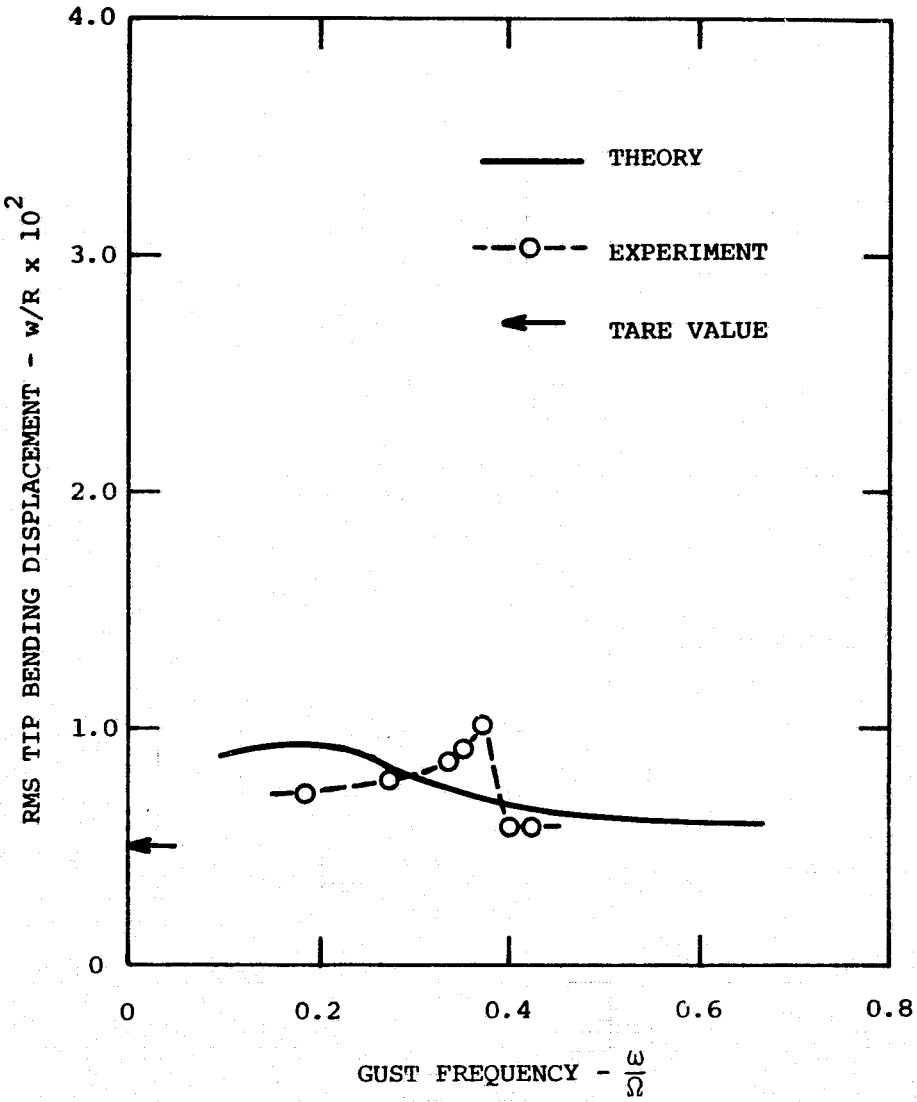

FIG. 6(b) VERTICAL GUST RESPONSE OF HINGELESS ROTOR BLADE OUT-OF-PLANE BENDING

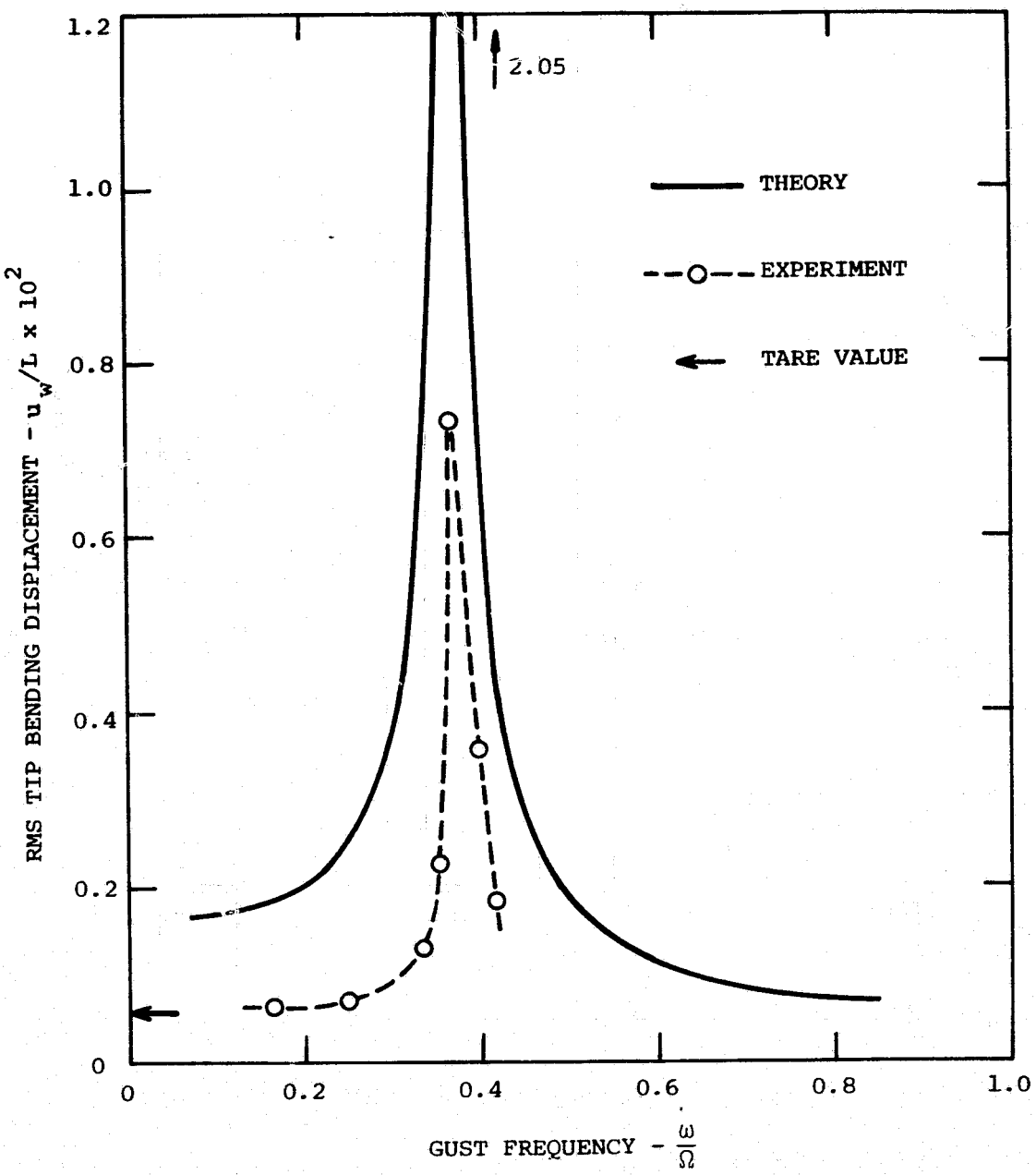

FIG. 6(c) VERTICAL GUST RESPONSE OF HINGELESS ROTOR WING VERTICAL BENDING

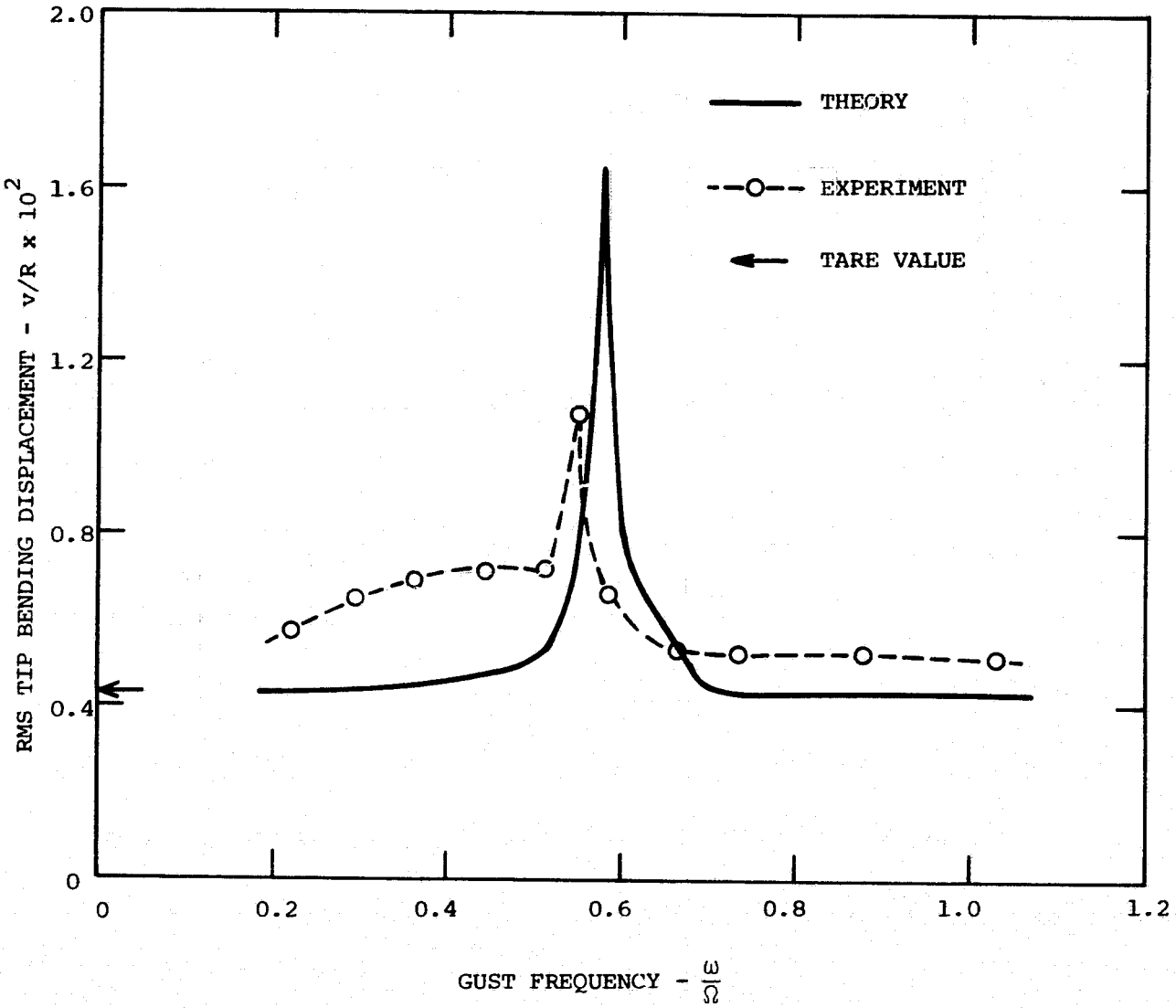

FIG. 7(a) LONGITUDINAL GUST RESPONSE OF GIMBALLED ROTOR BLADE INPLANE BENDING

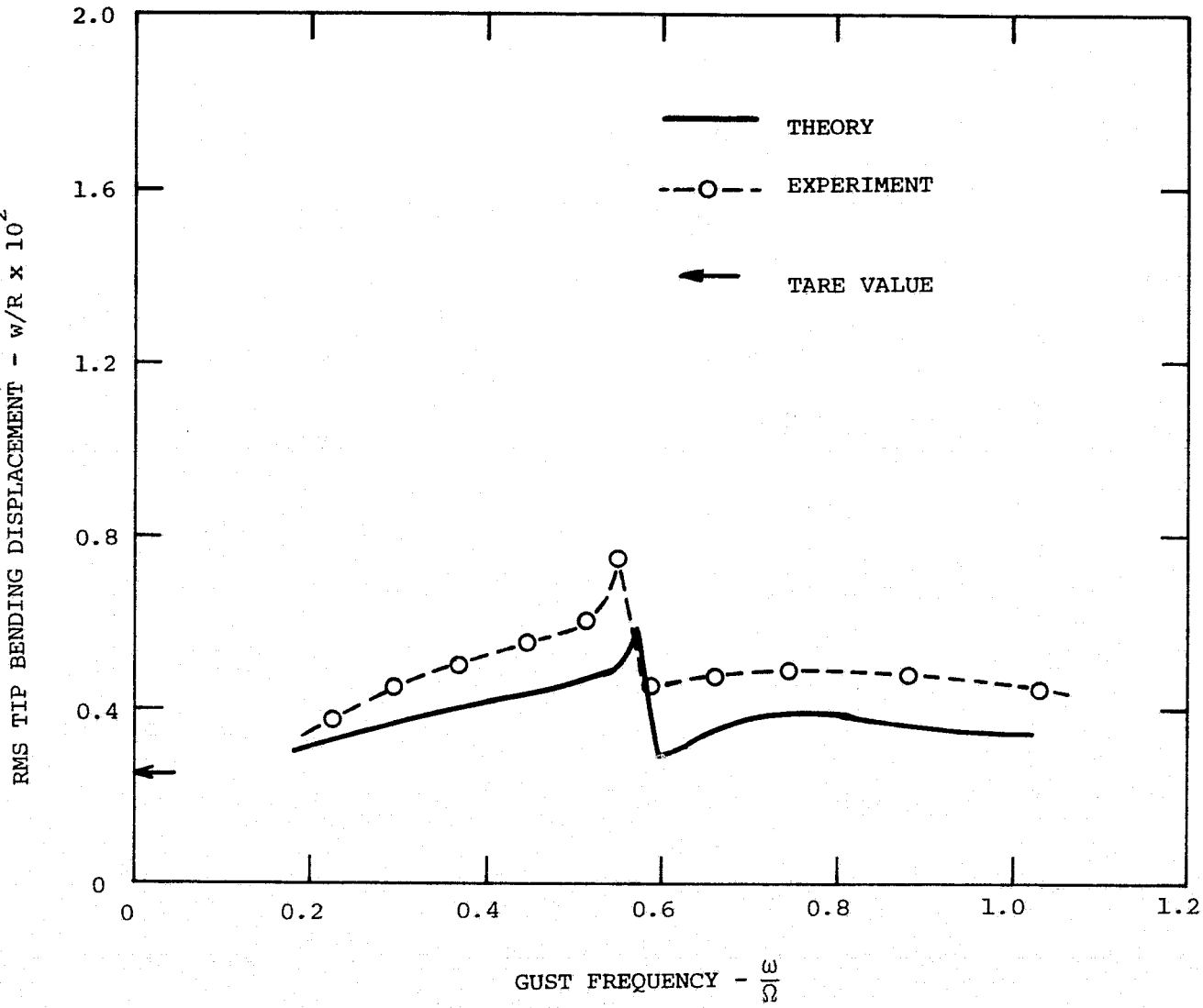

FIG. 7(b) LONGITUDINAL GUST RESPONSE OF GIMBALLED ROTOR BLADE OUT-OF-PLANE BENDING

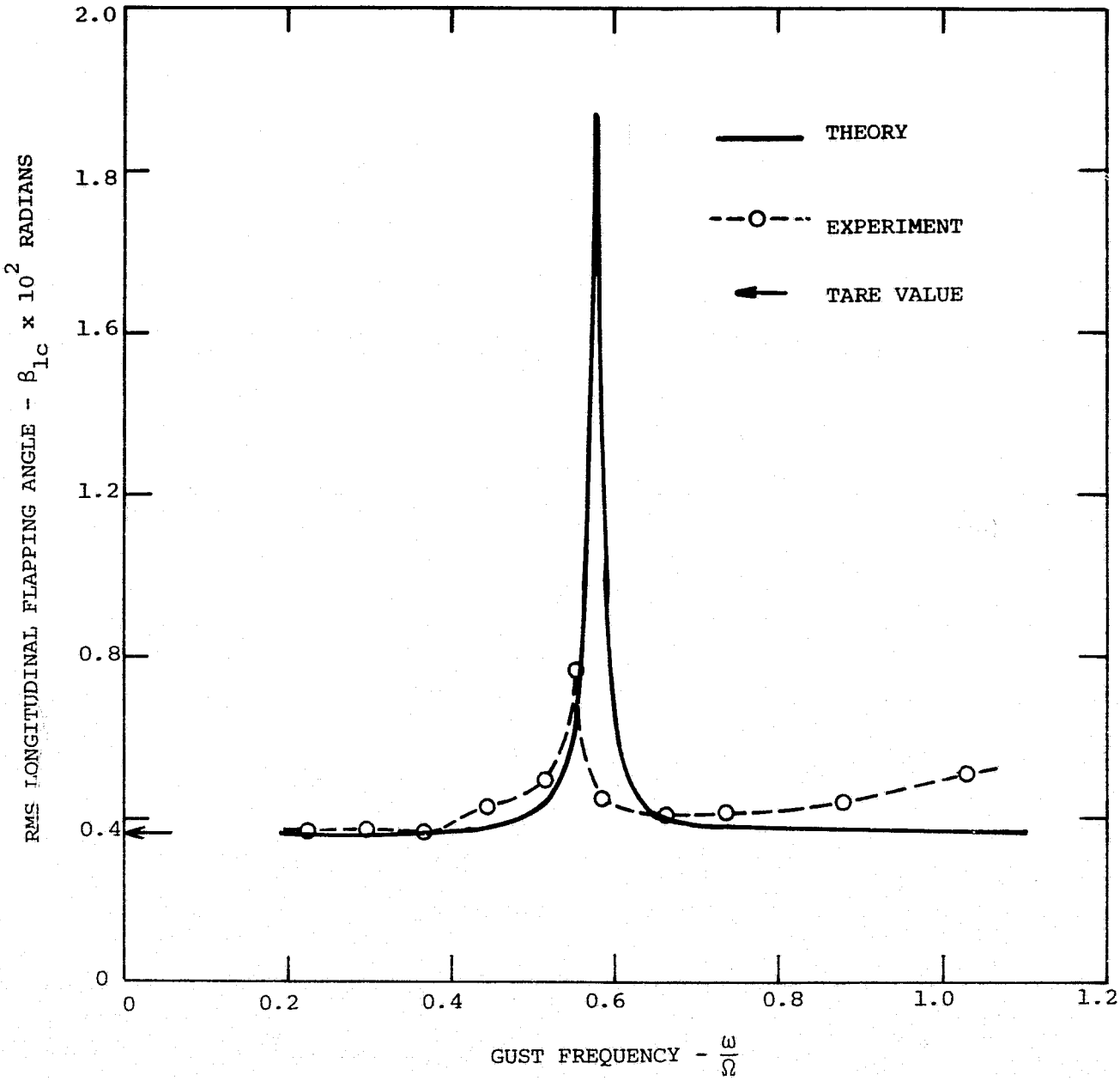

FIG. 7(c) LONGITUDINAL GUST RESPONSE OF GIMBALLED ROTOR LONGITUDINAL FLAPPING

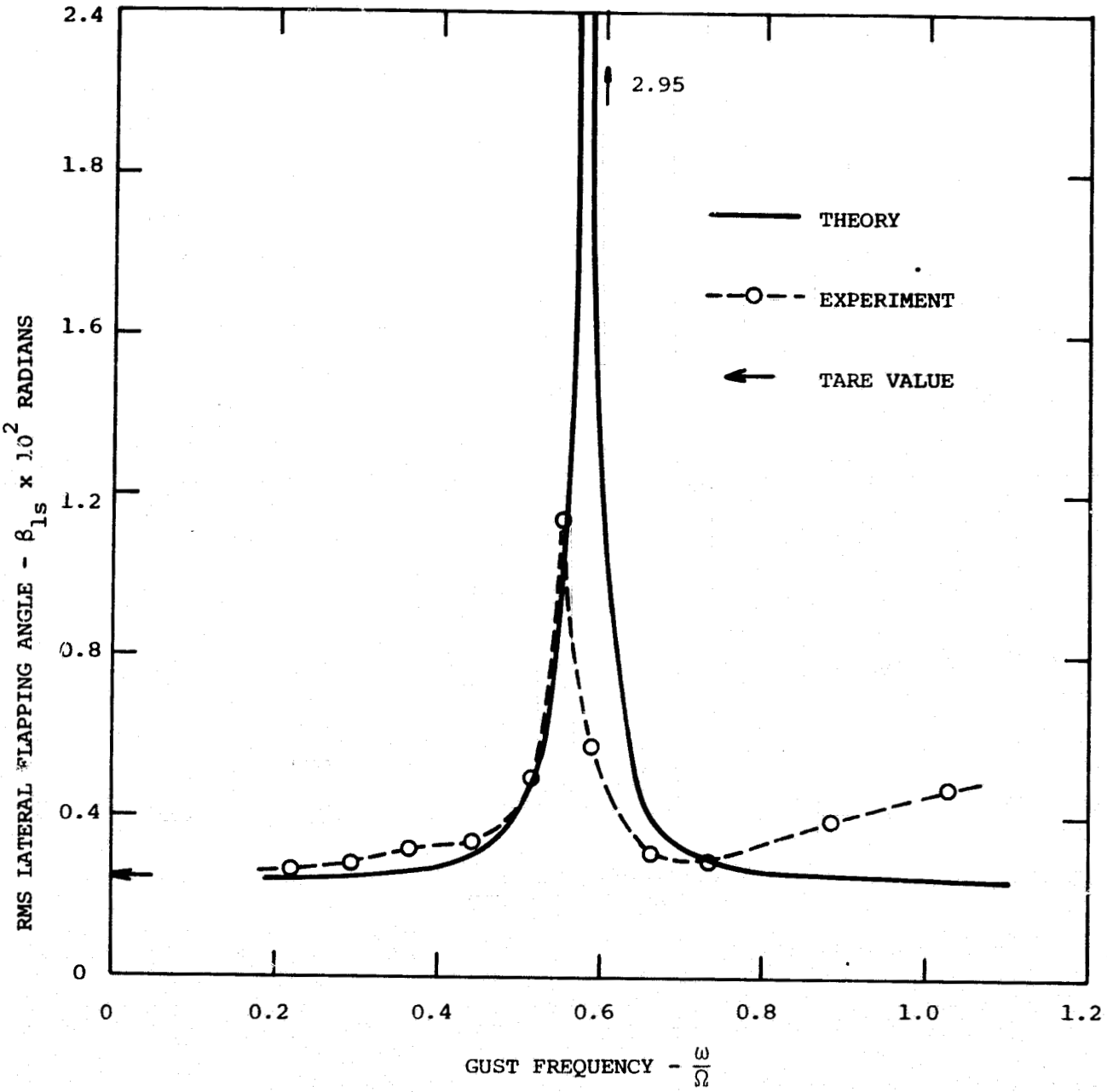

FIG. 7(d) LONGITUDINAL GUST RESPONSE OF GIMBALLED ROTOR LATERAL FLAPPING

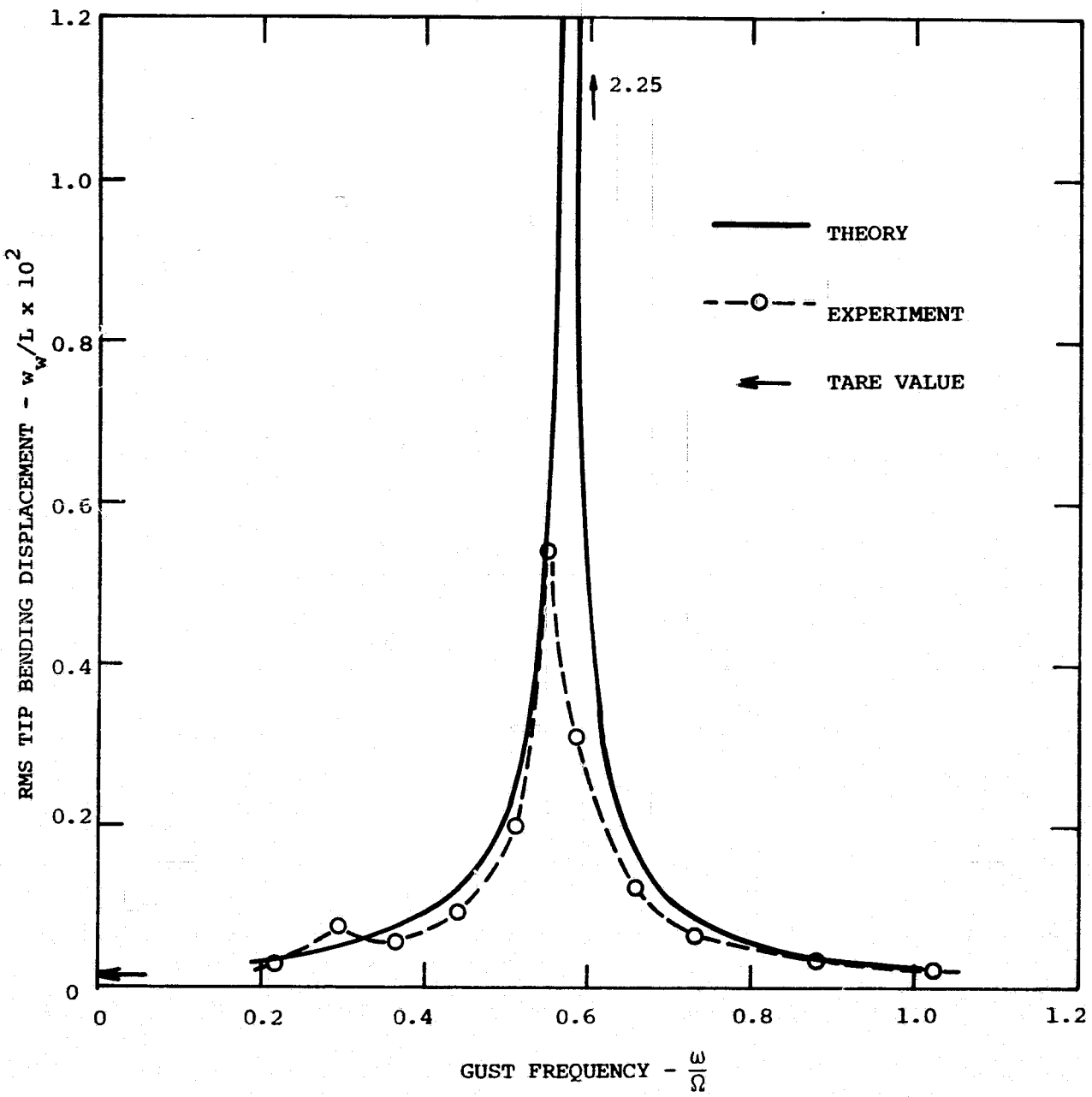

FIG. 7(e) LONGITUDINAL GUST RESPONSE OF GIMBALLED ROTOR WING CHORDWISE BENDING

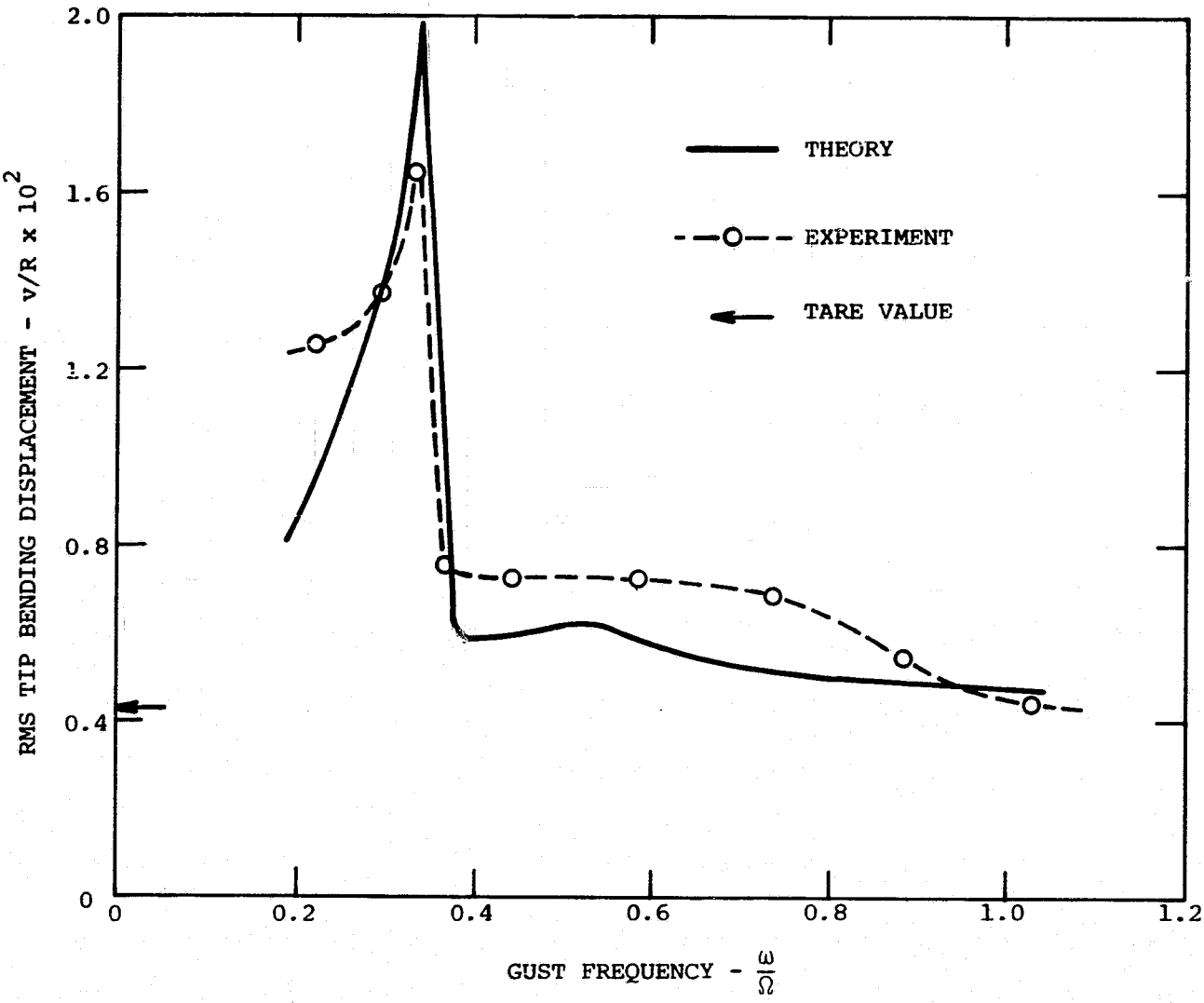

FIG. 8(a) VERTICAL GUST RESPONSE OF GIMBALLED ROTOR BLADE INPLANE BENDING

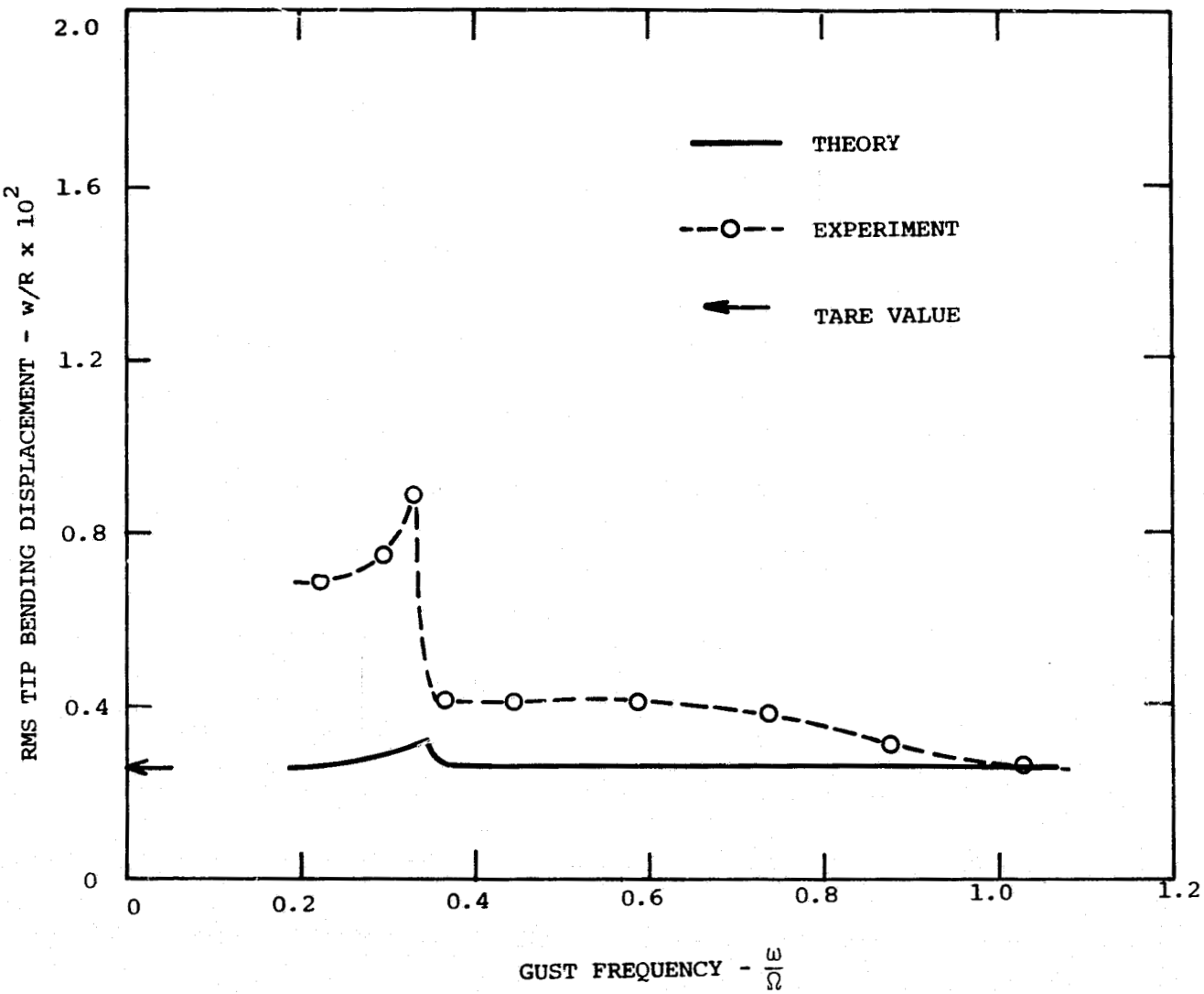

FIG. 8(b) VERTICAL GUST RESPONSE OF GIMBALLED ROTOR BLADE OUT-OF-PLANE BENDING

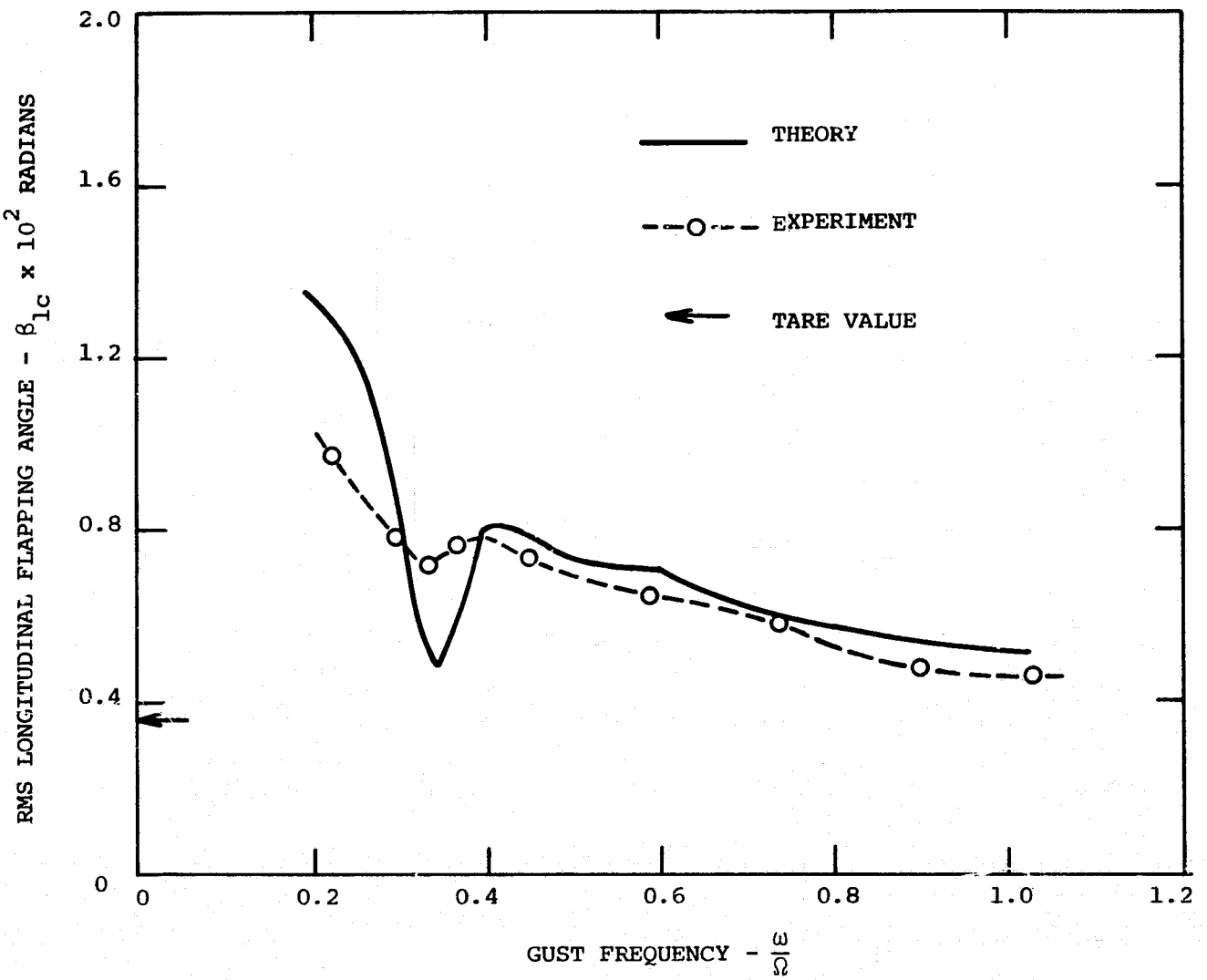

FIG. 8(c) VERTICAL GUST RESPONSE OF GIMBALLED ROTOR LONGITUDINAL FLAPPING

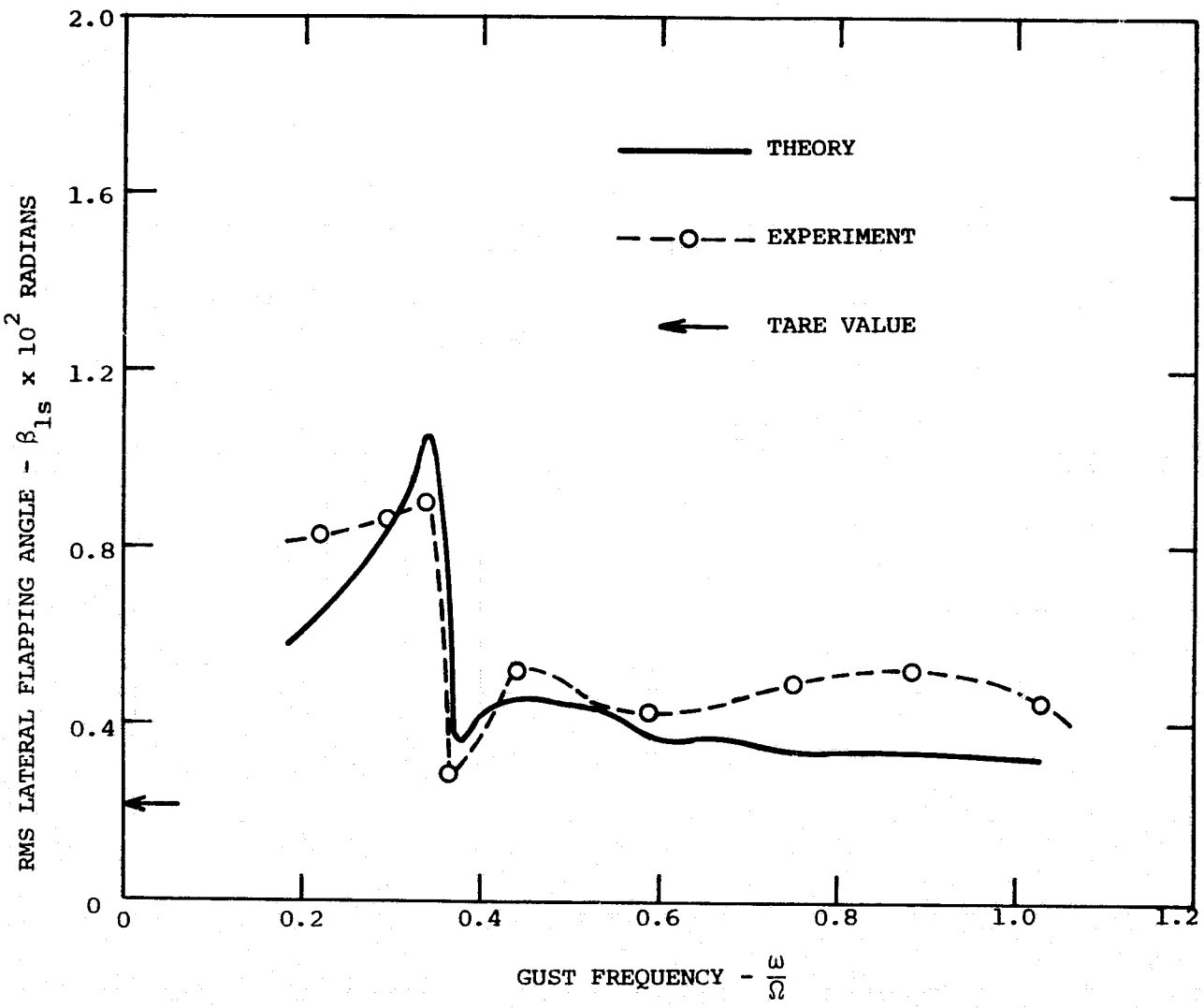

FIG. 8(d) VERTICAL GUST RESPONSE OF GIMBALLED ROTOR LATERAL FLAPPING

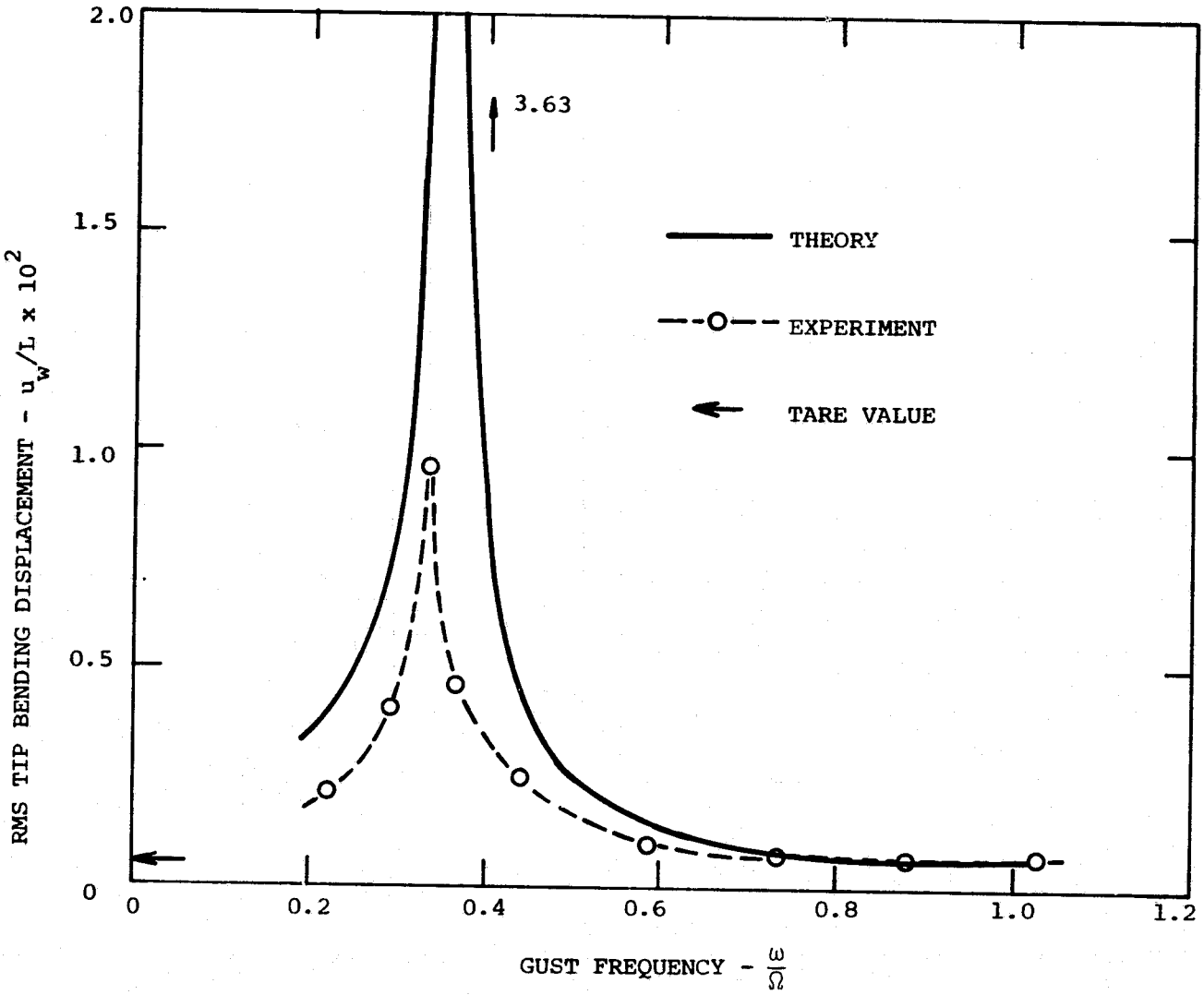

FIG. 8(e) VERTICAL GUST RESPONSE OF GIMBALLED ROTOR WING VERTICAL BENDING

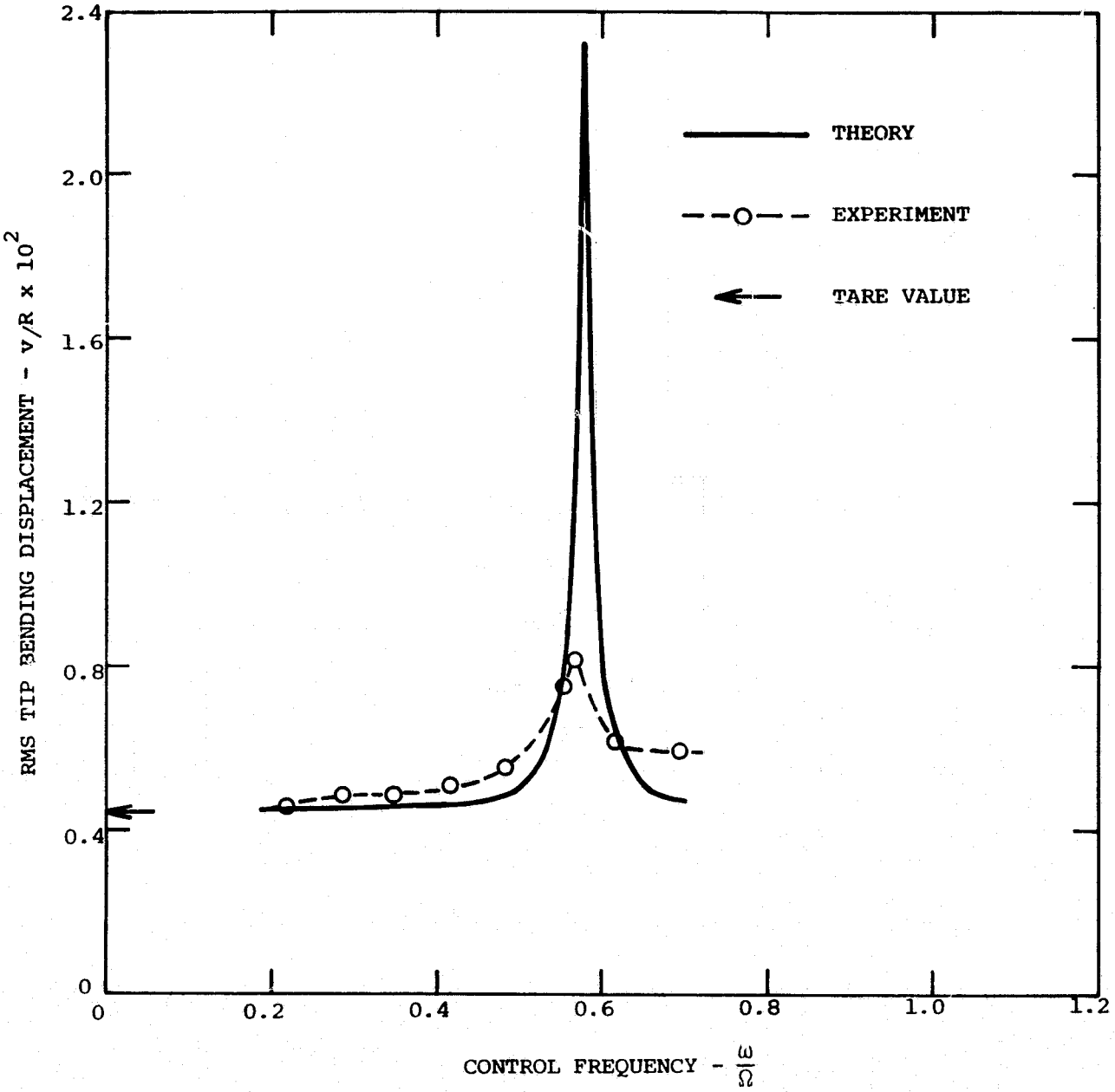

FIG. 9(a) COLLECTIVE PITCH CONTROL RESPONSE OF GIMBALLED ROTOR BLADE INPLANE BENDING

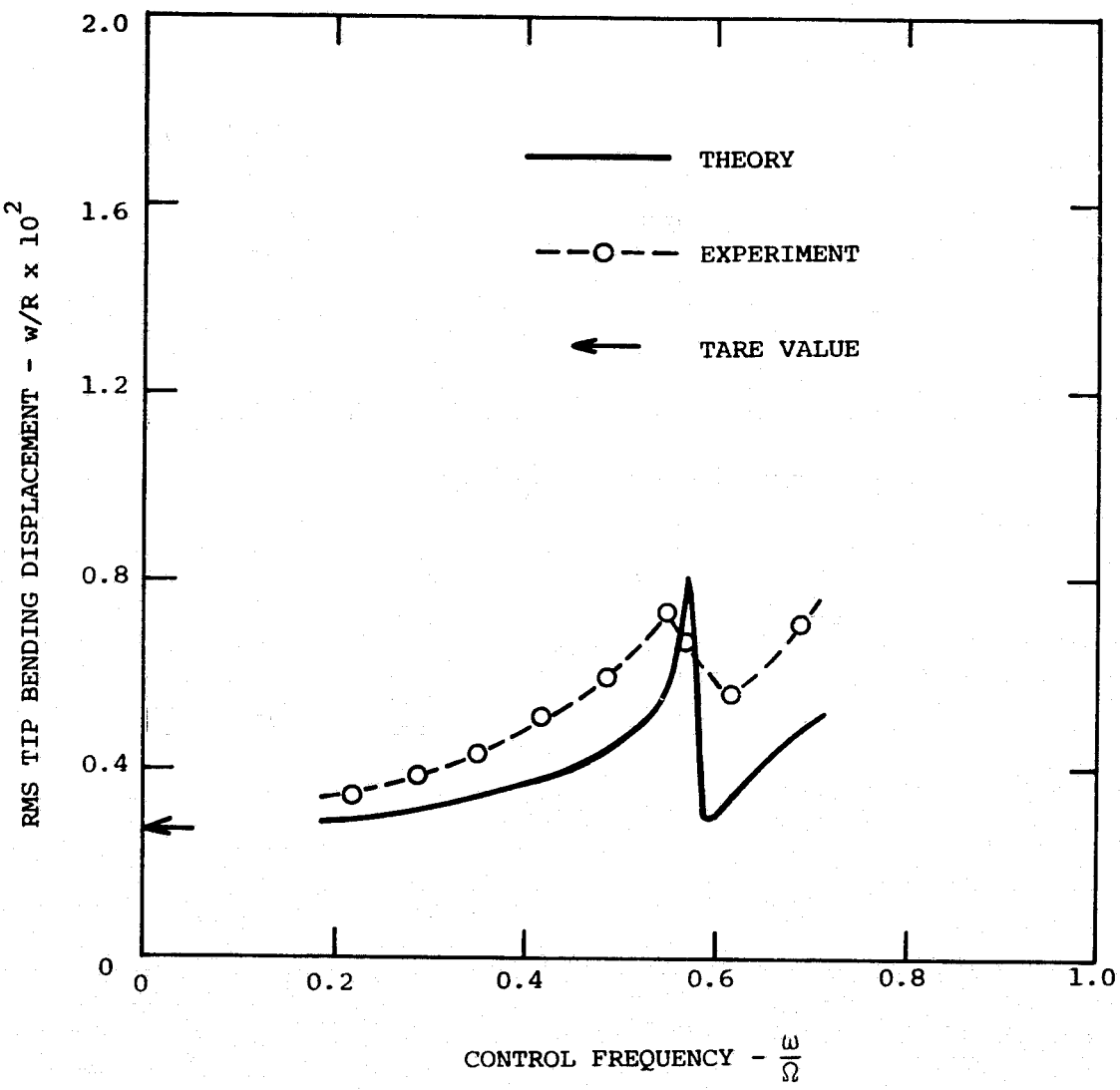

FIG. 9(b) COLLECTIVE PITCH CONTROL RESPONSE OF GIMBALLED ROTOR BLADE OUT-OF-PLANE BENDING

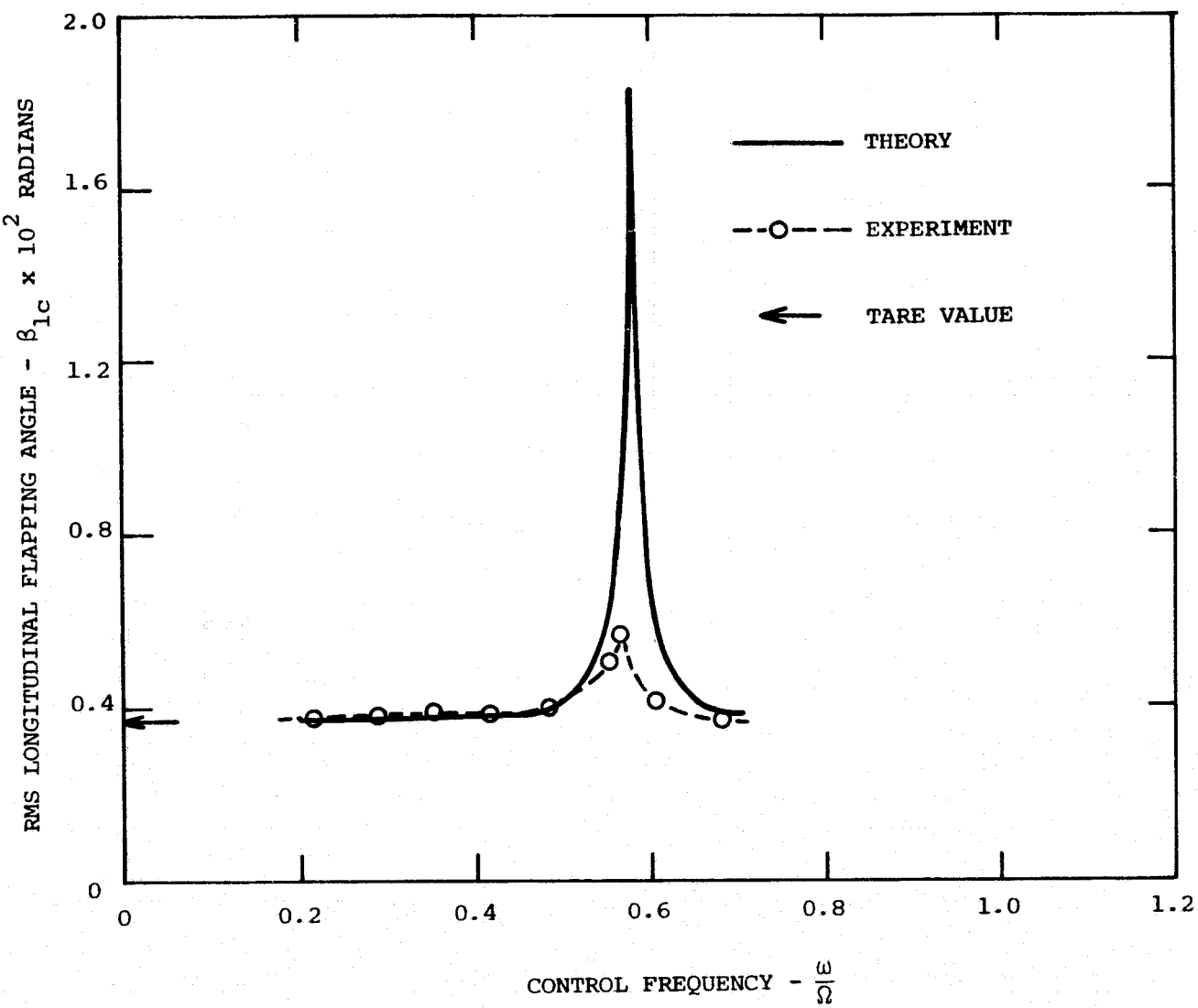

FIG. 9(c) COLLECTIVE PITCH CONTROL RESPONSE OF GIMBALLED ROTOR - LONGITUDINAL FLAPPING

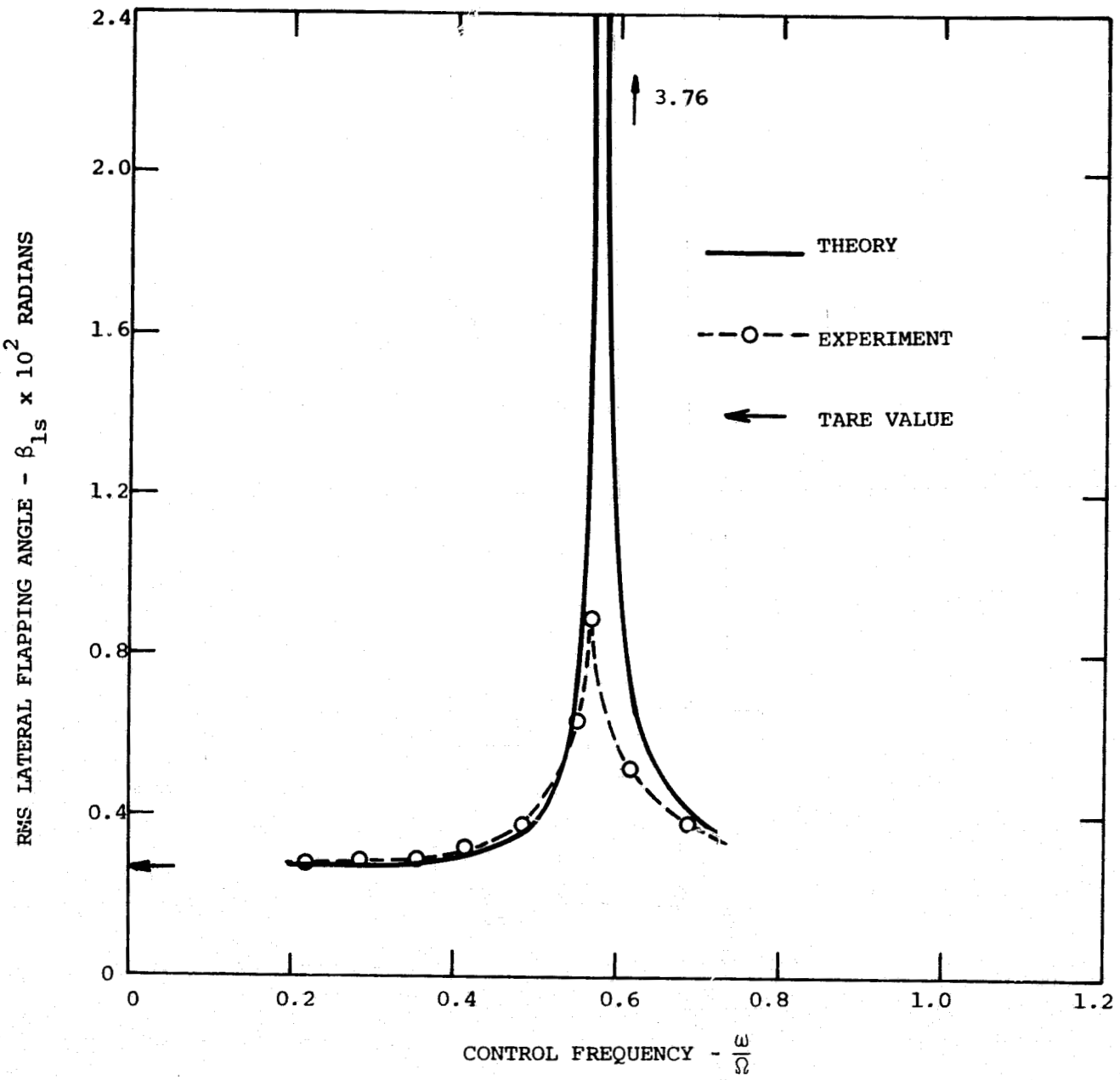

FIG. 9(d) COLLECTIVE PITCH CONTROL RESPONSE OF GIMBALLED ROTOR - LATERAL FLAPPING

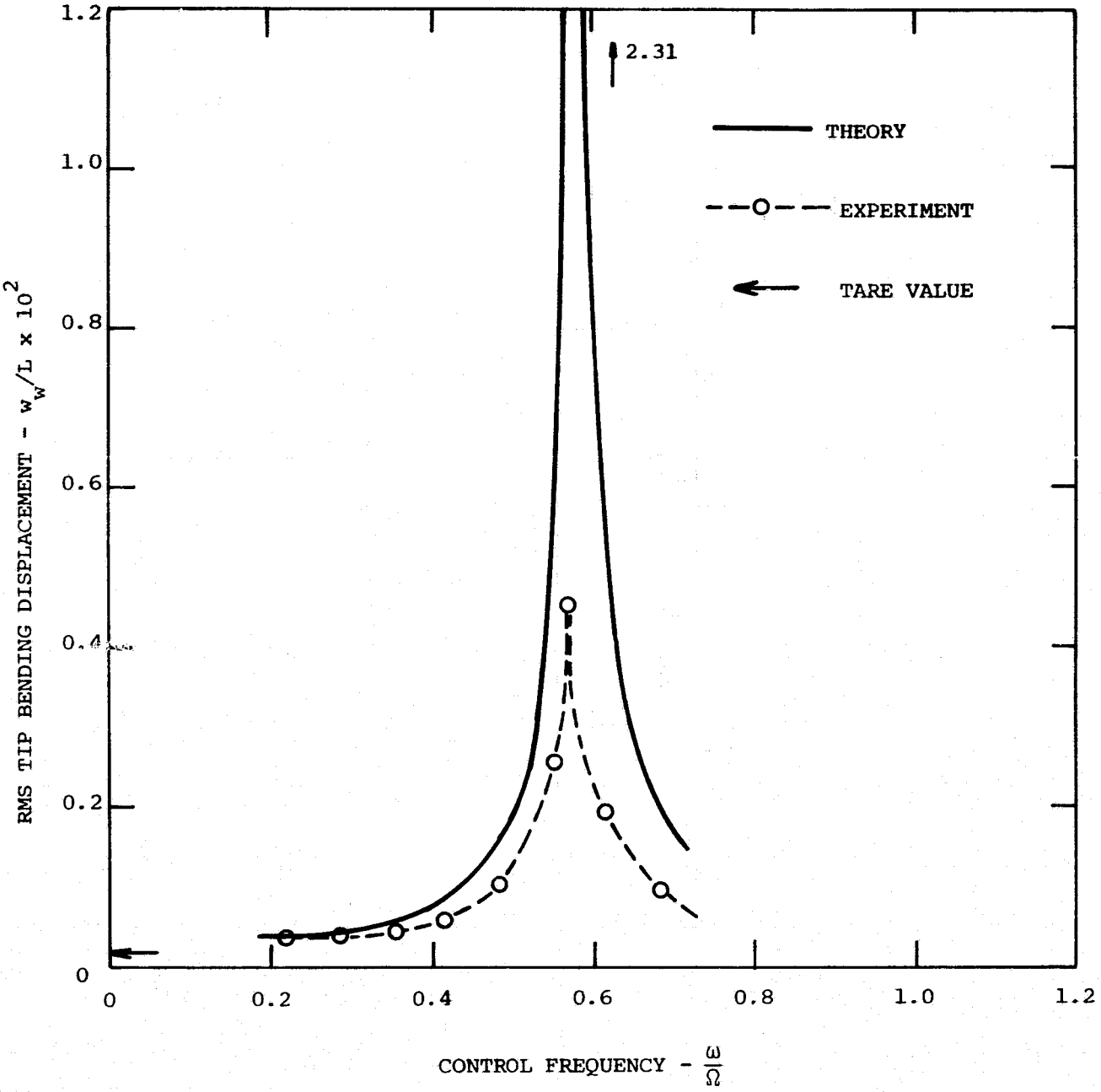

FIG. 9(e) COLLECTIVE PITCH CONTROL RESPONSE OF GIMBALLED ROTOR - WING CHORDWISE BENDING

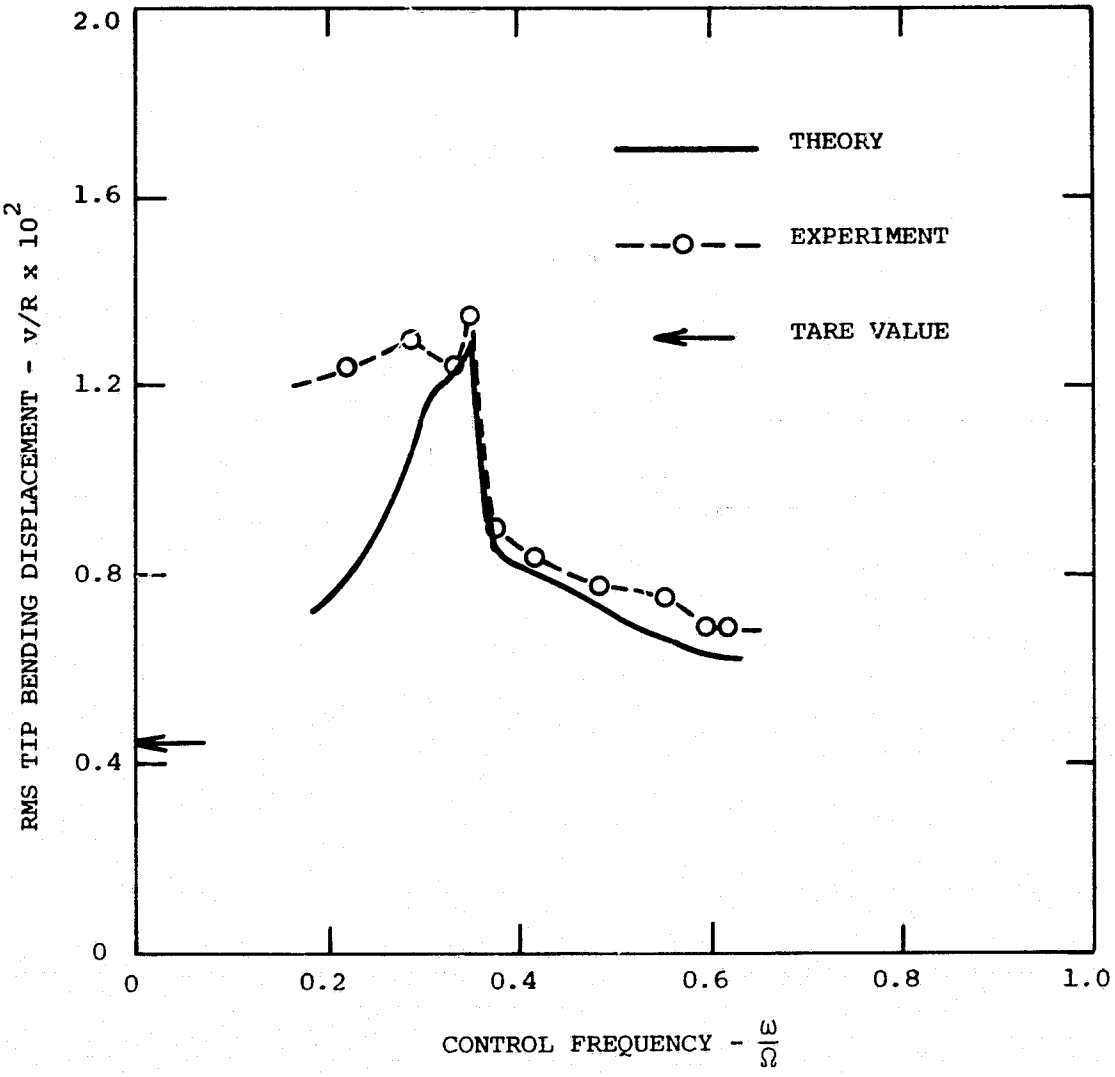

FIG. 10(a) CYCLIC PITCH CONTROL RESPONSE OF GIMBALLED ROTOR
ROTOR - BLADE INPLANE BENDING

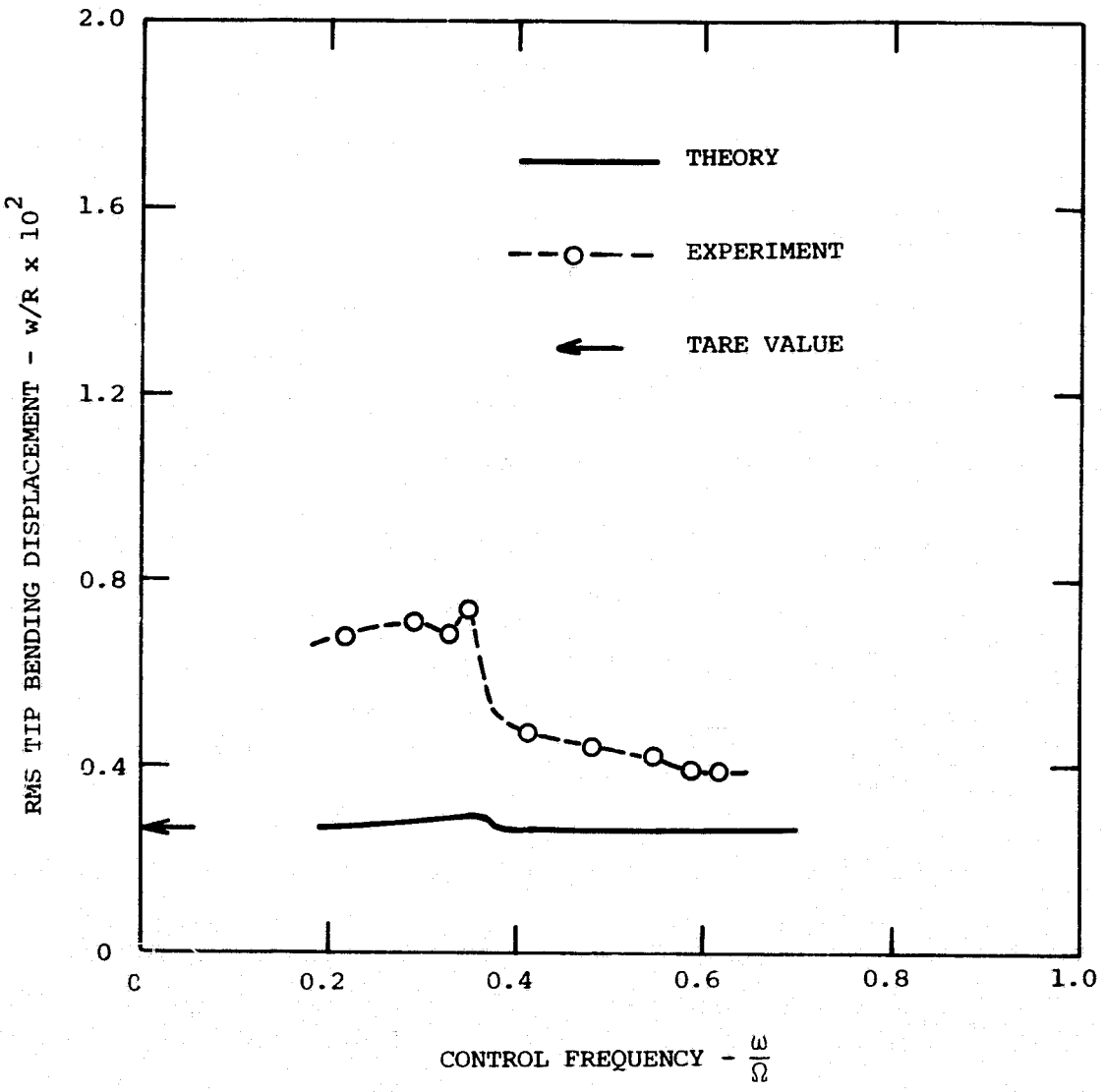

FIG. 10(b) CYCLIC PITCH CONTROL RESPONSE OF GIMBALLED ROTOR - BLADE OUT-OF-PLANE BENDING

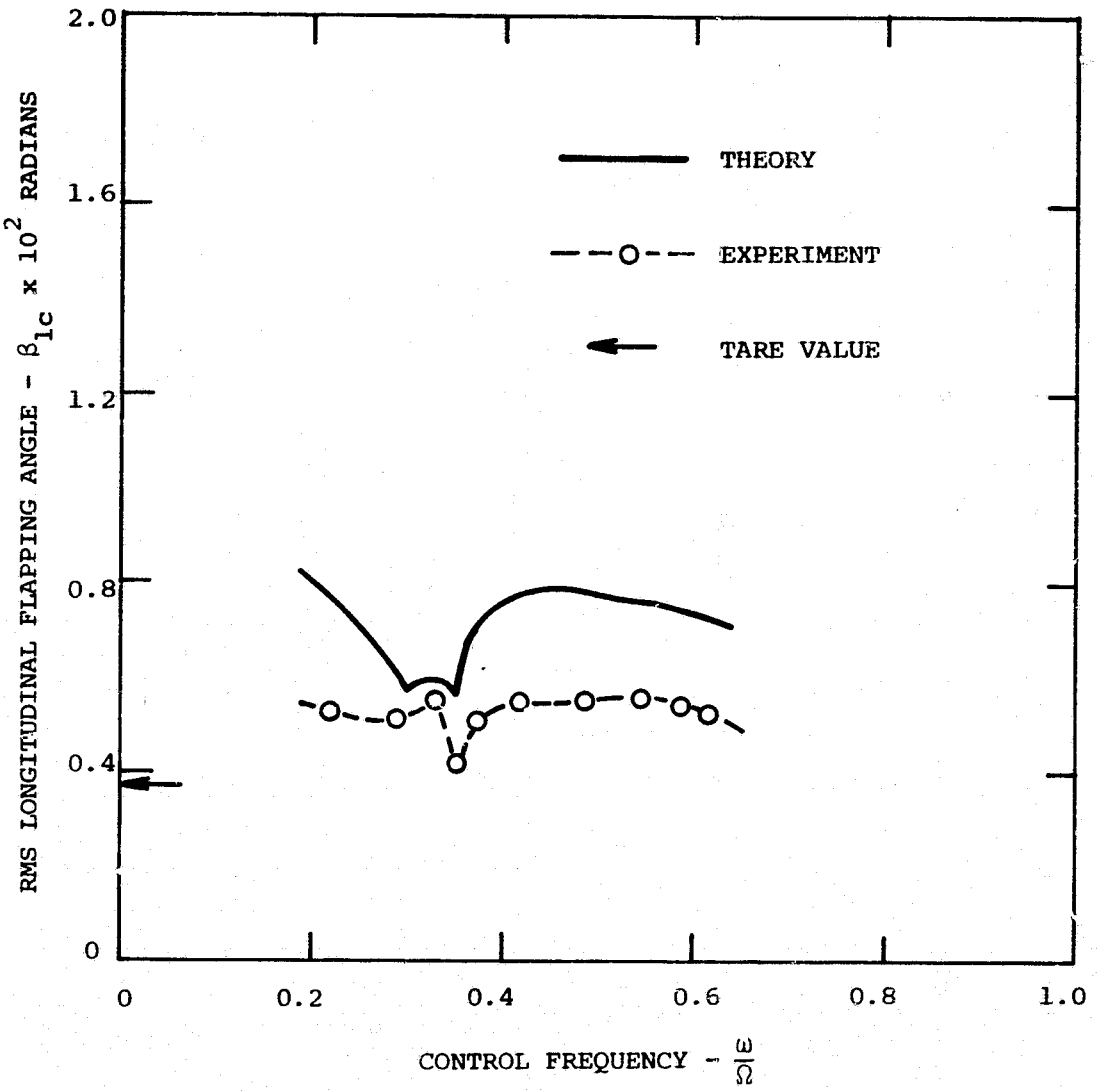

FIG. 10(c) CYCLIC PITCH CONTROL RESPONSE OF GIMBALLED ROTOR - LONGITUDINAL FLAPPING

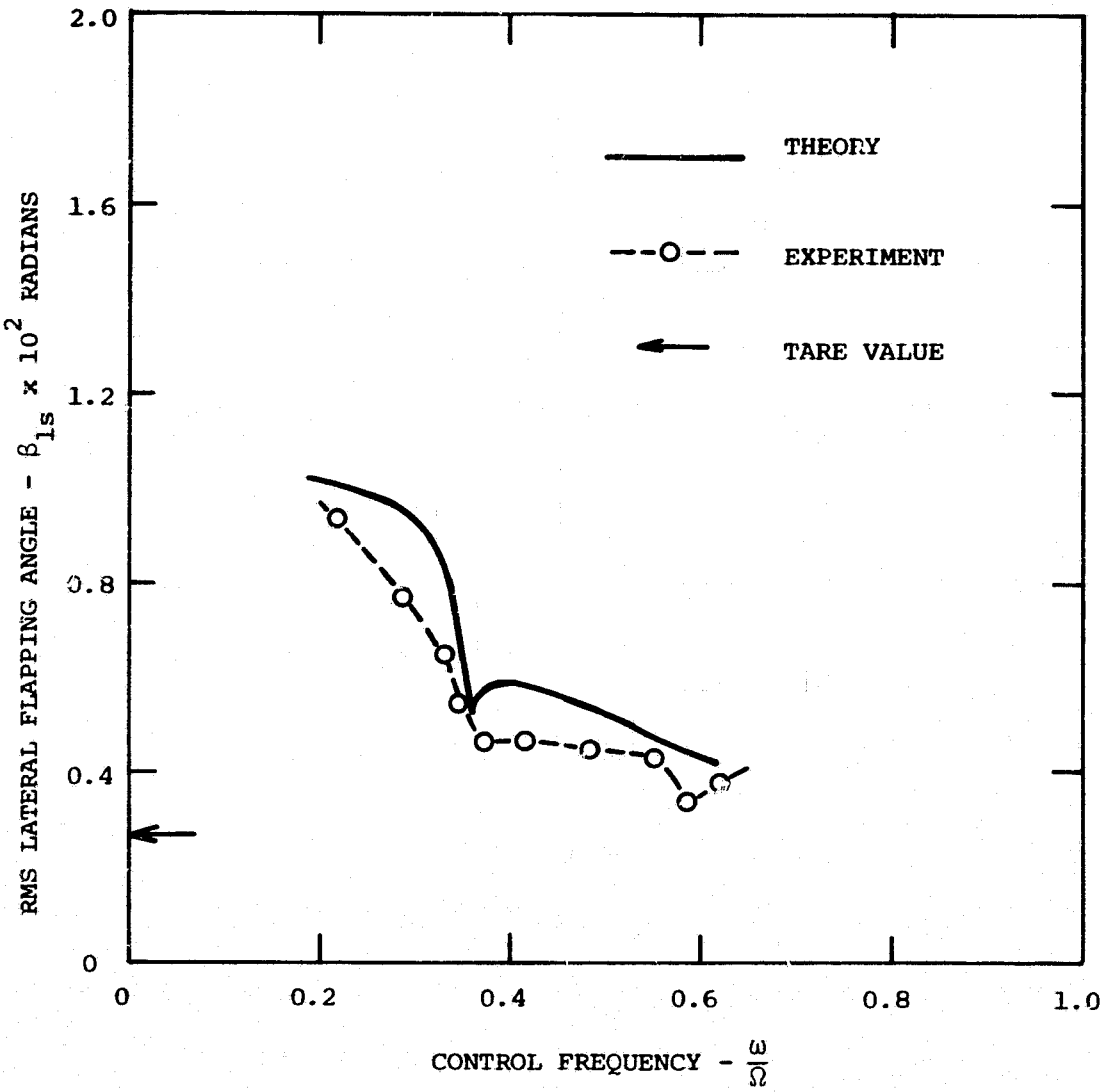

FIG. 10(d) CYCLIC PITCH CONTROL RESPONSE OF GIMBALLED ROTOR - LATERAL FLAPPING

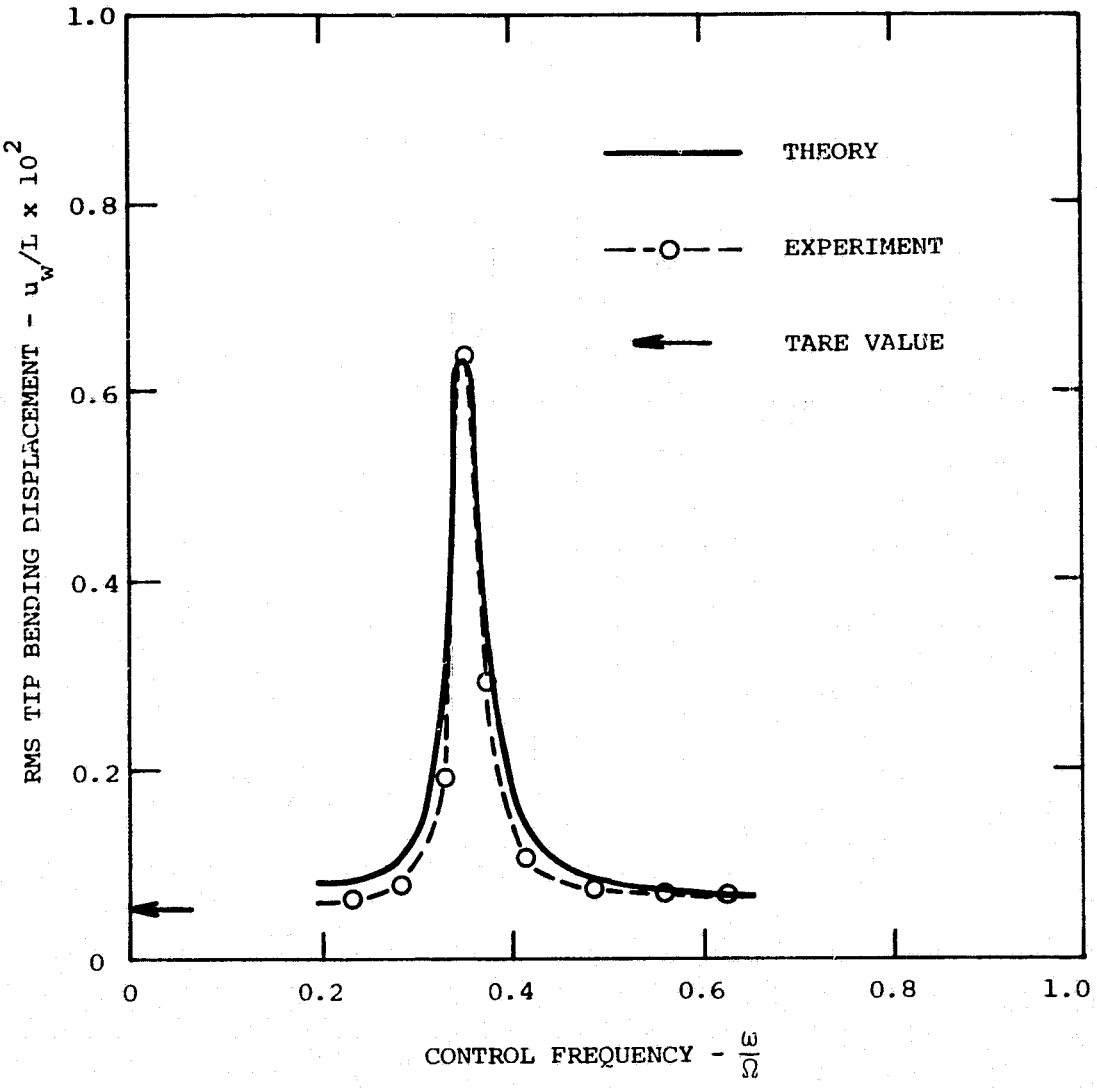

FIG. 10(e) CYCLIC PITCH CONTROL RESPONSE OF GIMBALLED ROTOR - WING VERTICAL BENDING

APPENDIX A

MODEL PARAMETERS

The model parameters are given in Table A-1 and in Reference 10.

The lift-curve slope and drag coefficients of the rotor and wing are estimated values.

Blade rotating natural frequencies were calculated using the program ROTOR described in Ref. 9. The same wing is used for both rotors. However, the natural frequencies with the rotor on are different due to different wing tip and rotor weights. The wing natural frequencies have most important roles in the proprotor dynamics; therefore to ensure those are accurately represented, the experimental wing frequencies are used in the theoretical analysis. The mass and stiffness distributions of the wing are employed to determine the wing mode shapes.

TABLE A-1

	GIMBALLED ROTOR MODEL	HINGELESS ROTOR MODEL
ROTOR		
Type	Gimballed, stiff in-plane	Cantilever, soft inplane
No. of Blades	3	3
Radius R	16.875 in.	16.875 in.
Chord	2.04 in.	2.04 in.
Lock number	4.63	5.80
Solidity	0.115	0.115
Pitch/Flap Coupling (delta three)	-11.8 deg	0
Lift-curve slope	5.7	5.7
Drag coefficient, C_{D_o}	0.0065	0.0065
Rotor Rotation Direction, looking forward	Clockwise	Clockwise
Blade Rotating Natural Frequencies at normal rotor rotational speed Ω		
Collective Mode		
First	1.84/rev (41.8 Hz)	1.30/rev (26.0 Hz)
Second	4.21/rev (95.3 Hz)	3.08/rev (61.6 Hz)
Cyclic Mode		
First	1.02/rev (23.2 Hz)	0.72/rev (14.4 Hz)
Second	1.37/rev (31.0 Hz)	1.31/rev (26.2 Hz)
Blade Flapping inertia	1.95×10^{-3} slug-ft^2	1.56×10^{-3} slug-ft^2
Weight of three Blades and Hub	0.775 lb	0.537 lb
Flapping Spring	25.0 in-lb/rad	0
Precone	1.5 deg	2.5 deg

TABLE A-1 CONCLUDED

	GIMBALLED ROTOR MODEL	HINGELESS ROTOR MODEL
WING		
Semispan L	23.2 in.	23.2 in.
Chord	6.7 in.	6.7 in.
Mast Height from the Wing Elastic Axis	5.054 in.	5.224 in.
Sweep	5.5 deg. forward	5.5 deg. forward
Dihedral	0	0
Lift-curve slope	5.7	5.7
Drag Coefficient, C_{D_o}	0	0
Aerodynamic Center	5.4% chord forward from the elastic axis	5.4% chord forward from the elastic axis
Natural Frequencies		
Vertical Bending	0.358/rev(8.10Hz)	0.372/rev (7.43Hz)
Chordwise Bending	0.582/rev(12.2Hz)	0.625/rev(12.5Hz)
Torsion	1.47/rev(33.3Hz)	1.82/rev(36.4Hz)
PYLON		
Weight	3.63 lb	3.63 lb
Yaw inertia	0.00731 slug-ft^2	0.00731 slug-ft^2
Pitch inertia	0.00731 slug-ft^2	0.00731 slug-ft^2
Roll inertia	0.001 slug-ft^2	0.001 slug-ft^2
Pylon C.G.	0.171 in behind the wing elastic axis	0.171 in behind the wing elastic axis